https://doi.org/10.5194/egusphere-2026-1696
Preprint. Discussion started: 19 May 2026

Evaluation of cloud base height provided by ceilometers and a proposal for a visibility-based quantitative definition for aviation

Daniel Klaus[1], Ulrich Görsdorf[1], Ranvir Dhillon[2], Joshua D. Vande Hey[2], and Julika Zinke[3, a]

[1]Meteorological Observatory Lindenberg, Deutscher Wetterdienst (DWD), Tauche (OT Lindenberg), Germany
[2]Earth Observation Science Research Group, School of Physics and Astronomy, University of Leicester, Leicester, UK
[3]Meteorological Institute, University of Hamburg, Hamburg, Germany
[a]now at: Baltic Sea Centre, Stockholm University, Stockholm, Sweden

Correspondence: Daniel Klaus (Daniel.Klaus@dwd.de)

Abstract. Ceilometers are established sensors for deriving cloud base height (CBH) from a laser backscatter signal. However, various types of ceilometers provide different CBHs for the same cloud situation due to the application of manufacturer-specific, proprietary algorithms and, above all, the lack of generally valid quantitative definition. This is particularly critical for air traffic control in low cloud situations. In the framework of the AutoMETAR project by Deutscher Wetterdienst (DWD) and in collaboration with the Universities of Leicester and Hamburg, the multiphase "**Cei**lometer **ca**mpaign **H**ansestadt **H**amburg" (CircaHH) was carried out. Across three measurement campaigns conducted between September 2016 and May 2019, primarily during the fall-spring seasons when low clouds are more prevalent, photographs of the 300 m tall "Hamburg Weather Mast" were taken for subsequent image analysis. Since the mast is increasingly obscured from the top downwards if the CBH descends, the contrast ratio of its alternating red and white segments was used to calculate the extinction coefficient profile. Several independent methods were analyzed for their suitability and accuracy to derive CBH from these extinction profiles. Our results suggest that the slant optical range (SOR) using a threshold value of 1000 m is an appropriate quantitative CBH definition for aviation, providing pilots with more useful information for an oblique downward or upward view. This SOR definition was also applied to extinction coefficient profiles derived from backscatter signals of different ceilometers using our own implementation of the Klett inversion method (KIM). This cross-check reveals that CBH differences due to various ceilometer backscatter input data for the KIM are significantly smaller than CBH differences associated with different ceilometer algorithms. Despite the complex experimental setup, our image analysis can serve as a new reference method for evaluating vertical profiles of the ceilometer backscatter signal for low clouds and can be used as a quality check for CBHs from any ceilometer firmware. Our KIM, combined with the SOR definition, has the potential to improve automated airport weather reports for CBH and cloud amount like routine Meteorological Aerodrome Report (METAR) and local routine report (MET REPORT).

https://doi.org/10.5194/egusphere-2026-1696
Preprint. Discussion started: 19 May 2026

1 Introduction

In aviation, visibility, distance from cloud and ceiling are the key factors governing the transition between a flight under visual meteorological conditions and instrument meteorological conditions (ICAO, 2024b). The pilot must identify the runway or runway approach lights by visibility at an angle of inclination corresponding to the glide slope of approximately 3°. If visibility is severely restricted, pilots may have to switch to instrument flight rules (IFR) and rely on both on-board instruments and air navigation service. In practice, aviation meteorologists and air traffic controllers use one or more vertically oriented ceilometers as a basis and complex cloud algorithms to estimate what the pilot should expect as cloud base height (CBH) for a specific airport. This makes misunderstandings sometimes virtually inevitable. Vertical visibility (VV), even though determined and provided as vertical optical range (VOR) by many ceilometers, is not the most suitable quantity for final landing approach. However, the visual range estimated from the critical height along the glide path or another oblique direction would be of more practical benefit, as already emphasized by Gaumet et al. (1998).

An important factor of flight safety is the ceiling, which indicates the height above ground level (AGL) of the lowest cloud layer with a cloud amount higher than $4\,\mathrm{oktas}$. According to the definition of the International Civil Aviation Organization (ICAO) in Annex 2 (ICAO, 2024a), this is "*the height above the ground or water of the base of the lowest layer of cloud below 6000* m *covering more than half the sky.*" CBH and ceiling are commonly given in feet rather than meter ($1\,\mathrm{ft} = 0.3048\,\mathrm{m}$), but both units are used here depending on the question and clarity. Airplane pilots, especially those flying commercial airliners, primarily operate under IFR. In contrast, the large majority of helicopter pilots fly according to visual flight rules (VFR). IFR and VFR are regionally specified, for example, in the Easy Access Rules for Standardised European Rules of the Air (EAR for SERA; EASA, 2024) by the European Union Aviation Safety Agency (EASA). This document also includes the categories for instrument approach operations according to ICAO (2022) and ICAO (2024b). The higher the category, the more restrictions there are for the pilot and the more financial losses can arise for the airport due to less frequent take-offs and landings. The rules for low visibility operations are specified by EASA (2025). Rescue helicopters in particular need accurate and reliable reports on current weather conditions, as rescue operations cannot be carried out in "significant weather" conditions (e.g. low ceiling and dense fog). Thus, the issue extends beyond financial considerations to matters of personal safety.

The cloud information, generated for pilots, aviation meteorologists, and air traffic controllers, is based on ceilometer data and is distributed as routine (METAR) or special (SPECI) Meteorological Aerodrome Report and corresponding local report (MET REPORT or SPECIAL) as described in ICAO (2018). All of these current airport weather reports have been determined and reported fully automatically at all 15 German international airports since 23 August 2022 (AutoMETAR project). Ceilometers are compact and cost-effective devices that exploit Light Detection And Ranging (LIDAR) technology and serve as the standard measuring system for deriving CBH and VOR from the backscatter coefficient profile. Neglecting multiple scattering, the relationship between the two unknowns (β = backscatter coefficient and σ = extinction coefficient) and the actually measured backscatter signal power

$$P(r,\lambda) = C_{\mathrm{L}}(\lambda)\frac{O(r,\lambda)}{r^2}\,\beta(r,\lambda)\,e^{-2\,\tau(r,\lambda)} + P_{\mathrm{bg}} \tag{1}$$

https://doi.org/10.5194/egusphere-2026-1696
Preprint. Discussion started: 19 May 2026

is described by the simplified lidar equation (Wandinger, 2005; ISO 28902-4, 2025), where $C_{\mathrm{L}}(\lambda)$ is the "lidar constant" that includes all system parameters (transmission power, efficiency of optics, etc.) partly as a function of wavelength, $O(r,\lambda)$ is the overlap function that corrects the incomplete overlap between the transmitted laser beam and the receiver's field of view, r is the distance between the ceilometer and the backscattering particles,

$$\tau(r,\lambda) = \int_0^r \sigma(r',\lambda)\,\mathrm{d}r' \tag{2}$$

is the optical depth and P_{bg} is the background signal. The different methods used by ceilometers to determine the CBH can be found in Vande Hey (2013, 2015).

A major challenge in deriving CBHs and/or VOR at a given time from vertical profiles of the range-corrected signal or attenuated backscatter (β_{att}) is the absence of a universally valid, quantitative definition of CBH and of clouds in general (Spänkuch et al., 2022; ISO 28902-4, 2025). The ceilometer inter-comparison campaign CeiLinEx2015 (Görsdorf et al., 2016) already dealt with the effects of different technical properties (optical configuration, wavelength, noise correction, etc.), different manufacturer-specific, proprietary algorithms and the lack of a generally accepted definition on the determination of the CBH. One of the key findings from Görsdorf et al. (2016) is that the CBH determined with different ceilometers varies from about 40 m for low, non-precipitating Stratus clouds, 70 m for non-precipitating Stratocumulus clouds to several 100 m or even a few 1 km for a Cumulunimbus cloud with temporary heavy rainfall. The wide spread of CBHs determined by different ceilometers is confirmed by a more recent study from Wagner et al. (2024). According to Attachment A of ICAO (2018) the operationally desirable accuracy of the measurement is ± 1 okta for cloud amount and ± 10 m up to 100 m AGL (± 10 % above 100 m AGL) for CBH. However, the above-mentioned CBH differences between various ceilometers are significantly larger.

CBH and VOR values provided by one or more ceilometers are input data for ceilometer-internal or autonomous cloud algorithms that calculate representative values for an airport. More precisely, such a cloud algorithm, e.g. "autoCLD" as part of autoOBS from DWD (unpublished C^{++} code) or "ampycloud" from MeteoSwiss (Python code by Vogt et al., 2024), uses the clouds drifting over ceilometers during a specific time interval to derive CBH, cloud amount and VV height that are representative for the whole airport (METAR/SPECI) or a specific runway threshold (MET REPORT/SPECIAL). Each of these parameters need to be reported taking into account all the requirements and rules of the ICAO (ICAO, 2018). While Illingworth et al. (2019) confirm that each ceilometer has its own strengths and weaknesses, no downstream cloud algorithm can correct erroneous values and artifacts from the ceilometer input data. The greatest potential for improvement in cloud reports, not only in aviation, is therefore to replace the current ceilometer algorithms by an algorithm with a standardized CBH definition.

The assessment of both the measured β_{att}-profile (or σ-profile from Klett inversion method (KIM)) and the CBH provided by a ceilometer requires a reference method as ground truth. A σ-profile can be measured by a Raman lidar. Two Raman lidars are operated at the DWD, the very powerful RAMSES system (Reichardt et al., 2012) at the Meteorological Observatory Lindenberg and the compact multi-wavelength lidar Polly$^{\mathrm{XT}}$ (Althausen et al., 2009) at the Meteorological Observatory Hohenpeißenberg. RAMSES operates at a wavelength (λ) of 350 nm, while Polly$^{\mathrm{XT}}$ operates at wavelengths of 355 nm, 532 nm, and 1064 nm, but no σ is available at 1064 nm. In contrast, λ used by ceilometers is in the range of $853-1064$ nm (see Table 1).

https://doi.org/10.5194/egusphere-2026-1696
Preprint. Discussion started: 19 May 2026

Taking into account Eq. (1) and the λ^{-4} dependence of the backscatter intensity with elastic (Rayleigh) scattering, the λ differences to the ceilometers are too large for a reasonable comparison. Neither of the two Raman lidars is primarily designed for the (routine) measurement or derivation of the σ-profile in low cloud situations. Therefore, both were excluded as a reference as well as other methods considered and we unfortunately realized that there is no reference method yet.

The wide range of CBH values derived from different ceilometers in the same cloud situation and the lack of a suitable reference instrument for low clouds were the starting point for CircaHH, a collaboration between DWD and the Universities of Leicester and Hamburg. During a total of three measurement campaigns with the experimental setup presented in Sect. 2, photos from the 300 m tall "Hamburg Weather Mast" (HH-WeatherMast) were taken with a digital camera (Sony α7). These photos form the basis for the image analysis described in Sect. 3, which results in the vertical profile of the extinction coefficient that in turn can be used to determine the visibility-based CBH using various methods (Sect. 4). These CBH values are then compared with those provided by the firmware of various ceilometers in order to find a possible quantitative definition of CBH among the analyzed methods that would be universally applicable and, in particular, would improve aviation requirements (Sect. 5). While the ceilometer CBHs are only used for a qualitative comparison, visibility measurements from sensors installed at 2 m, 175 m and 280 m are used to assess the quality and accuracy of the extinction coefficient profile derived from image analysis. Could our image analysis even be suitable as an independent ceilometer reference method for very low clouds? The CBH definition we consider most suitable is additionally tested on σ-profiles derived directly from the β_{att}-profiles of various ceilometers using our own implementation of the KIM (Appendix A). Our conclusions are summarized in Sect. 6.

Finally, we want to mention that all participating ceilometer manufacturers: OTT HydroMet (incl. Lufft), Vaisala, and Campbell Scientific received a confidential version of our manuscript and gave their consent to the publication of the data and results.

2 Experimental setup and data

During all phases of CircaHH (see Table 1) we utilize the broadcast tower of a German television station (NDR) located in Hamburg. As this tower is equipped for meteorological measurements by the University of Hamburg and the DWD also uses the instruments, it is commonly referred to as "Hamburg Weather Mast" (HH-WeatherMast). It is 300 m tall and has 14 red and 13 white (i.e. a total of 27) alternating, non-equidistant segments.

The tower is increasingly obscured from the top downwards when the CBH descends. This obscuration and the increases and decreases in CBH are recorded using photos taken with a digital camera (Sony α7), which is located 178 m from the mast and 2 m less in the third CircaHH phase, as explained in the caption to Table 1. The photos pertaining to the work described here were taken with 1-minute temporal resolution (more details in Sect. 3) and are used to determine CBH values, which could then be compared with the CBH derived from ceilometers.

An increasing number of ceilometers were deployed on the test measuring field with a distance of ca. 30 m to 40 m to (close to) the tower. In total, we operated the following ceilometers of different manufacturers: CHM15k (Lufft, 2022a), CL31 (Vaisala, 2009), CS135 (Campbell, 2014), LD40 (Vaisala, 2005), CS136 (Campbell, 2018, replaced CS135) and CHM8k (Lufft, 2022b), where more details are summarized in Table 1.

https://doi.org/10.5194/egusphere-2026-1696
Preprint. Discussion started: 19 May 2026

Table 1. Overview of ground-based measuring instruments and sensors installed on the Hamburg Weather Mast used during the **three phases of CircaHH**. The time format is YYYYMMDD, manufacturer's names appear in italic font and the laser wavelength (λ) of any ceilometer is given in brackets. The present weather sensor CS125 was replaced by PWS100 on 11 January 2017. The sky camera was installed on 22 November 2017. The distance of the Sony α7 to the mast was 178 m during phases one and two but 176 m during the third phase, since a new camera was installed and reoriented on 26 September 2018. The measurements used from the mast were carried out in 2 m, 10 m, 50 m, 70 m, 110 m, 175 m, 250 m, 280 m height (HH-WeatherMast). The two PWD20 visibility sensors in 175 m and 280 m were only installed on 08 March 2018.

Phase	**Data time period**		**Measuring instruments**	
	Start	End	ground-based	on mast
1	20160926	20170421	Camera: *Sony* α7 (ILCE-7)	Temperature: *Ludwig Schneider* Pt100
			Ceilometer: *Lufft* CHM15k "NIMBUS" (1064 nm)	Humidity: *Vaisala* Humicap
			Vaisala CL31 (910±10 nm)	
			Campbell Scientific CS135 (905 nm)	
			Visibility: *Campbell Scientific* CS125	
			Campbell Scientific PWS100	
2	20171116	20180925	Camera: *Sony* α7 (ILCE-7)	Temperature: *Ludwig Schneider* Pt100
			Ceilometer: *Lufft* CHM15k "NIMBUS" (1064 nm)	Humidity: *Vaisala* Humicap
			Vaisala CL31 (910±10 nm)	Visibility: *Vaisala* PWD20
			Campbell Scientific CS135 (905 nm)	
			Vaisala LD40 (855±2 nm)	
			Visibility: *Campbell Scientific* PWS100	
			Sky camera: *Mobotix* SkyView	
3	20180928	20190520	Camera: *Sony* α7 (ILCE-7)	Temperature: *Ludwig Schneider* Pt100
			Ceilometer: *Lufft* CHM15k "NIMBUS" (1064 nm)	Humidity: *Vaisala* Humicap
			Vaisala CL31 (910±10 nm)	Visibility: *Vaisala* PWD20
			Campbell Scientific CS136 (912±5 nm)	
			Vaisala LD40 (855±2 nm)	
			Lufft CHM8k (905 nm)	
			Visibility: *Campbell Scientific* PWS100	
			Sky camera: *Mobotix* SkyView	

In addition to the ceilometers a present weather sensor CS125 (Campbell, 2016), which was later replaced by a more powerful PWS100 (Campbell, 2015), recorded measurement data of horizontal visibility according to Eq. (12) in Sect. 4. A sky camera was installed at the beginning of the second CircaHH phase and helped in particular for the detection of cloud hit false alarms. Two visibility sensors of type PWD20 (Vaisala, 2004) were installed at 175 m and 280 m height in spring 2018. These mea-

https://doi.org/10.5194/egusphere-2026-1696
Preprint. Discussion started: 19 May 2026

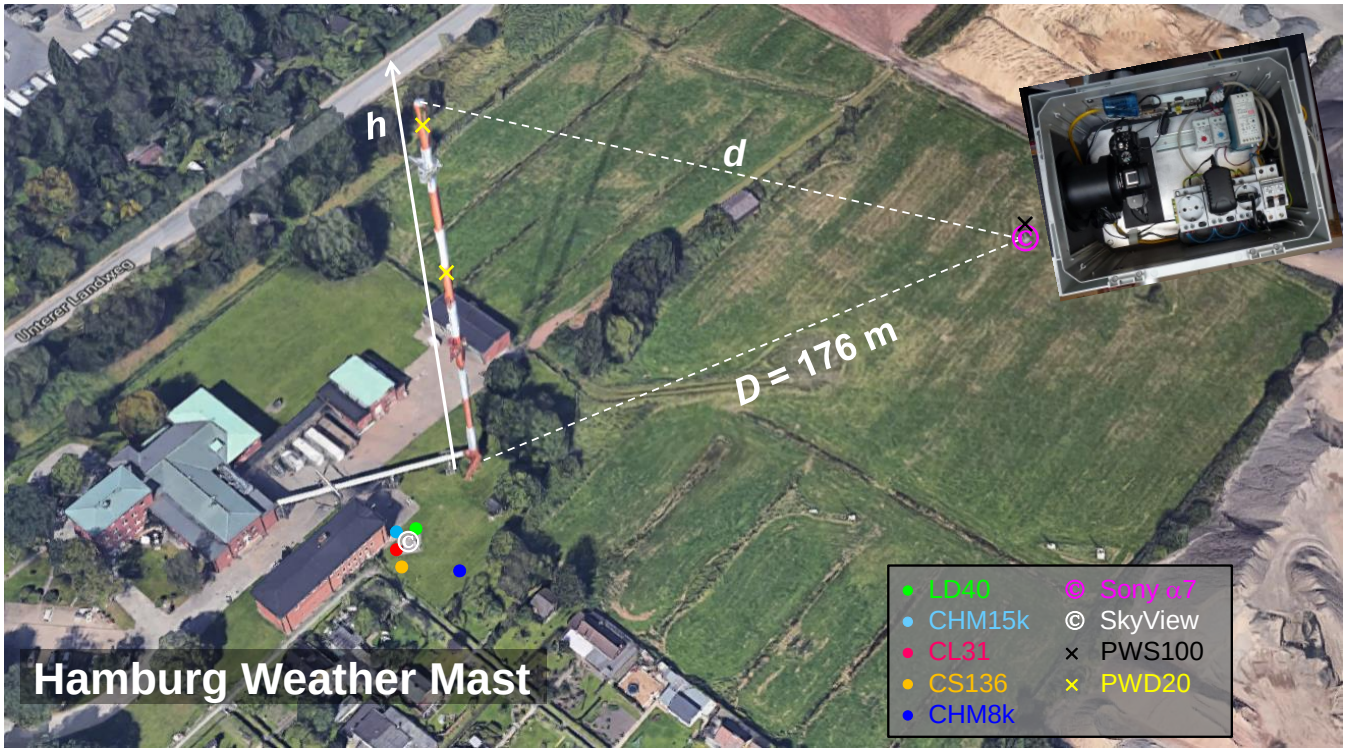

Figure 1. Sensors used during the third CircaHH phase (see Table 1) as part of the international tender for finding a new ceilometer type at German international airports. This elaborate and unique experimental setup was build up at the 300 m tall NDR broadcast tower in Hamburg, where additional meteorological instrumentation (e.g. temperature and humidity sensors) is used by University of Hamburg to operate the so-called "Hamburg Weather Mast" (HH-WeatherMast). Map data: © Google (2019).

surements should help to evaluate the vertical profiles of the extinction coefficient derived from image analysis.

The entire range and arrangement of sensors used during the third CircaHH phase is illustrated in Fig. 1. This setup was used as part of the AutoMETAR project during the international tender (data basis: from 28 September 2018 to 31 January 2019) to replace and renew the ceilometers at German international airports. All the data obtained, the increasingly sophisticated experimental setup and our growing knowledge helped us to finally formulate a quantitative definition for CBH as described in the next sections.

3 Image analysis

As mentioned in Sect. 2 the Sony $\alpha 7$ with a wide-angle lens was installed at least 176 m away from the Hamburg Weather Mast. In this way, the camera's field-of-view included the entire tower. However, image analysis was performed starting at about 14 m height (see *white scale* in Fig. 2(b)) to avoid artifacts caused by vegetation (trees). If CBH was lower than 500 m

https://doi.org/10.5194/egusphere-2026-1696
Preprint. Discussion started: 19 May 2026

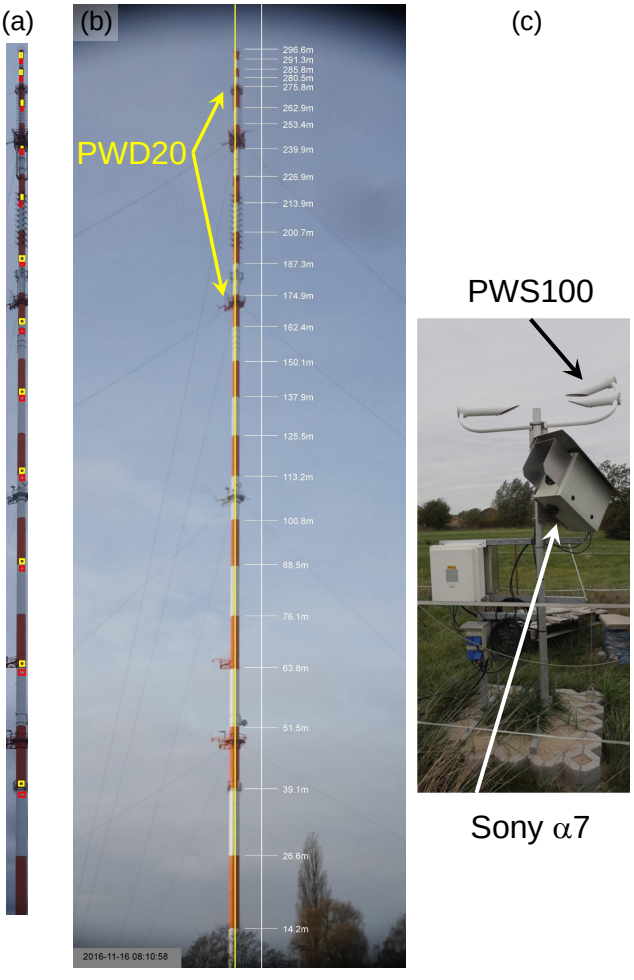

Figure 2. Primary measuring instruments used to perform and evaluate the image analysis. **(a)** Illustration of the assignment of rectangles to delimit a red-white segment pair on the Hamburg Weather Mast. These rectangles have different sizes, as the mast width decreases with increasing height; **(b)** Height values (*white scale*) from theodolit measurements are slightly inaccurate near the mast top. The non-equidistant mast segments are on average about 12.5 m long and the first platform is in 50 m height; **(c)** The camera and one of the three visibility sensors, which were installed about 180 m from the mast (see Fig. 1).

then a photo was taken every 1 min and otherwise every 10 min. This criterion was applied to the lowest CBH derived by all currently used ceilometers. The series of photos can be used either for visual verification or as the basis for an image analysis explained below in order to be able processing a longer dataset by objective criterions.

The photos (JPEG) provided by the Sony $\alpha 7$ are sRGB images that contain R'G'B' values for each pixel. This original data is read into an array L of pixel luminances and all entries are divided by 255 to obtain floating point values $(0.0 \leq L \leq 1.0)$, which means $(0,0,0)$ = black and $(1,1,1)$ = white. The mapping of these luminances into intensities (I) requires a non-linear

https://doi.org/10.5194/egusphere-2026-1696
Preprint. Discussion started: 19 May 2026

transfer function. The mapping function

$$I = \begin{cases} \frac{L}{12.92} & \text{for } L \leq 0.04045 \\ \left(\frac{L+0.055}{1.055}\right)^{\gamma} & \text{for } L > 0.04045 \end{cases} \tag{3}$$

with $\gamma = 2.4$ gives linear intensity values (RGB) and is the same for all channels (Wikipedia). Greyscale luminances were initially tried (Zinke, 2016) but found to be less suitable. Our final choice of the blue portion is most effective to distinguish between the red and white segments of the Hamburg Weather Mast.

The image analysis used in this study is therefore based on luminances of the blue channel that allows the assignment of start and end height of any red or white segment of the Hamburg Weather Mast. Where possible, rectangular cutouts of the mast from various sizes (30×40 to 20×15 pixels in Fig. 2(a)) were used to obtain average luminance values of 12 pairs of red and white segments. This was done in order to obtain representative luminance values that were reasonably accurate. The use of smaller rectangles was necessary in order not to include struts and lights on the mast, which tapers from bottom to top, complicating matters.

Intensities of consecutive red and white segments (each pair of red/white segment luminance values) allow the calculation of the Michelson contrast

$$C_n = \begin{cases} \frac{I_{n+1}}{I_n} - 1 & \text{for red/white transition} \\ \frac{I_n}{I_{n+1}} - 1 & \text{for white/red transition} \end{cases} \tag{4}$$

with $n = 1 \ldots 27$ (14 red and 13 white segments). C_n is normalized by the contrast value of the lowest red/white pair to take into account the given visual conditions. Otherwise, low clouds would appear lower when visibility is restricted compared to when visibility is unrestricted. As the pixel color values of a white segment are higher than those of a red segment, negative values can result in the first term of the right-hand side of Eq. (4), which requires a reciprocal formulation. Finally, the contrast values are interpolated vertically to 1 m resolution, they are then also available between the segment transitions.

The Michelson contrast C is determined for "apparent" (perceived) conditions when the mast is e.g. partially obscured by clouds and then related to the "inherent" (actual) Michelson contrast C_0 when there are no low-lying clouds and unobscured visibility or ideally clear sky conditions. Following Eq. (10) of Eberhard (1986)

$$\frac{C}{C_0} = e^{-\int_0^d \sigma(s)\,\mathrm{d}s} \tag{5}$$

and assuming the extinction coefficient is constant along the optical path ($\sigma(s) = \text{const.}$), its vertical profile can be derived successively from the ratio between apparent and inherent contrast values at a certain height (h) via

$$\sigma_{\mathrm{cs}}(h) = -\frac{\ln\left(\frac{C(h)}{C_0(h)}\right)}{d} \quad . \tag{6}$$

The subscript cs = "constant sigma" in Eq. (6) refers to the assumed constancy of the extinction coefficient and following the Pythagorean theorem

$$d = \sqrt{D^2 + H^2} \tag{7}$$

https://doi.org/10.5194/egusphere-2026-1696
Preprint. Discussion started: 19 May 2026

denotes the oblique line-of-sight distance between the Sony $\alpha 7$ and the actual height H of the point being viewed on the mast. We applied **two different approaches**:

A) Calculation of the $\sigma_{\mathrm{cs}}(h)$-profile using Eq. (6) with the usual constancy assumption for the extinction coefficient from the ground up to a certain height and application of different methods to derive CBH, which are described in Sect. 4.

B) Calculation of a variable extinction coefficient profile (vs = "variable sigma") assuming a linear relationship to the optical path s

$$\sigma_{\mathrm{vs}}(h) = m\,s + \sigma_0 \tag{8}$$

from the ground up to a certain height. Following Eq. (6.2) of Weitkamp (2005) the average oblique visual range between the two points at the camera and mast can be expressed by

$$\bar{V} = -\frac{d}{\int_0^d (m\,s + \sigma_0)\,\mathrm{d}s} \cdot \ln\left(\frac{C}{C_0}\right) \tag{9a}$$

$$= -\frac{d}{\frac{m}{2}\,d^2 + \sigma_0\,d} \cdot \ln\left(\frac{C}{C_0}\right) \quad . \tag{9b}$$

Here we assumed $\bar{V} = d$. This assumption is legitimate, since other visual ranges, for example MOR defined by Eq. (12), are also only distances for a specific contrast threshold value. Rearraging the Eq. (9b) to m gives a calculation rule

$$m = \frac{2}{d}\left[-\frac{\ln\left(\frac{C(h)}{C_0(h)}\right)}{d} - \sigma_0\right] \tag{10}$$

for the slope in Eq. (8), which can finally be rewritten as follows:

$$\sigma_{\mathrm{vs}}(h) = 2\,\sigma_{\mathrm{cs}}(h) - \sigma_0 \quad . \tag{11}$$

This approach is only applied to the MOR and SOR definitions introduced in Sect. 4 as these methods have been identified as the most suitable candidates, as will be shown later.

In Eq. (11) σ_0 is the extinction coefficient at the mast bottom. It was derived from the horizontal visibility measurements carried out with the PWS100 or CS125 and using Eq. (12). The fact that the visibility sensor was installed almost 180 m away from the mast is not a problem, as horizontal homogeneity of the extinction coefficient can be assumed. Further details on approach B) are given by Zinke (2016).

Regardless of the application of Eq. (6) or Eq. (11) the profile of the extinction coefficient was calculated with a vertical resolution of about 25 m and an even higher resolution of 1 m was achieved by linear interpolation. Figures 3(a−e) summarize the necessary steps to obtain $\sigma_{\mathrm{cs}}(h)$ or $\sigma_{\mathrm{vs}}(h)$ based on image analysis and show the results exemplarily for the 04 November 2018 at 10:30 UTC.

https://doi.org/10.5194/egusphere-2026-1696
Preprint. Discussion started: 19 May 2026

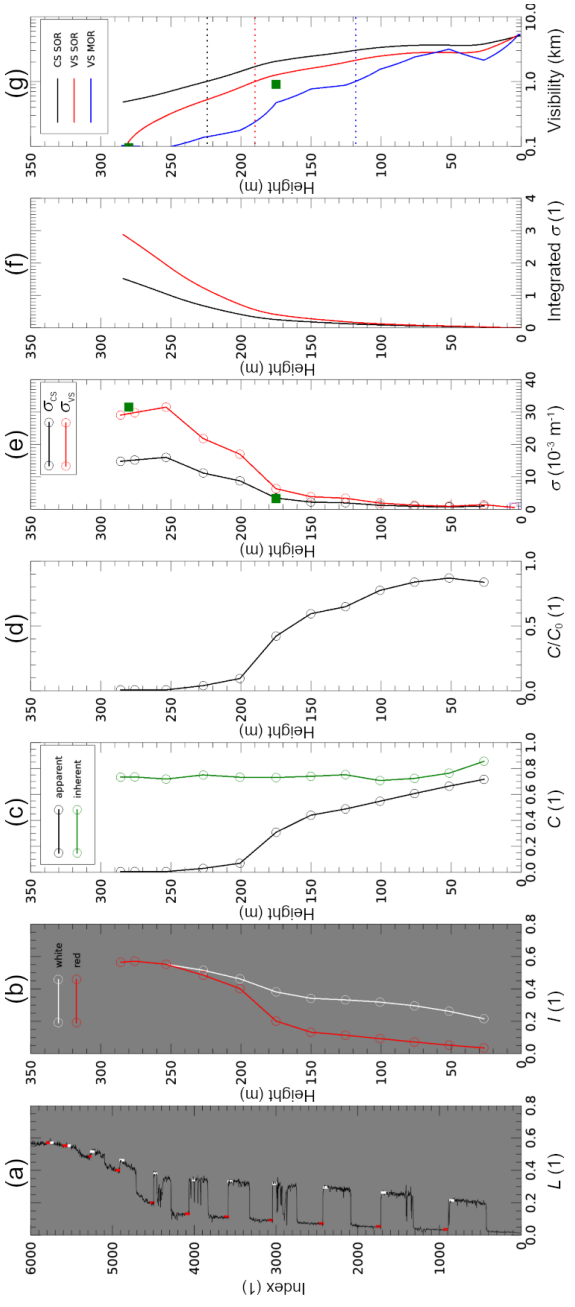

Figure 3. Step-by-step illustration of the image analysis and determination of CBH for 04 November 2018 at 10:30 UTC: **(a)** Assignment of red and white segments to luminance L of the blue channel; **(b)** Determine intensity I of consecutive red and white segments; **(c)** Calculate Michelson contrast values C for "apparent" (perceived) and "inherent" (no clouds $\leq 300\,\mathrm{m}$ and unobscured horizontal visibility) conditions; **(d)** Calculate contrast ratio C/C_0; **(e)** Determine the vertical profile of $\sigma_{\mathrm{cs}}(h)$ using Eq. (6) or $\sigma_{\mathrm{vs}}(h)$ using Eq. (11); **(f)** Calculate the integral over the extinction coefficient profile; **(g)** Apply threshold value of $1000\,\mathrm{m}$ to MOR or SOR definition to finally determine CBH (*horizontal dashed lines*). The indices "CS" and "VS" mean "constant sigma" and "variable sigma" according to approach A) and B) in Sect. 3. The green squares show results from the PWD20 in $175\,\mathrm{m}$ and $280\,\mathrm{m}$ height.

https://doi.org/10.5194/egusphere-2026-1696
Preprint. Discussion started: 19 May 2026

4 Attempts to define CBH

The following independent methods are tested to determine the CBH based on image analysis:

- **RW CONT**: Not using the extinction coefficient, this method searches for the height at which the ratio C/C_0 equals 5 % as recommended by WMO and ICAO (ICAO, 2005).
- **CS GRAD**: Using σ_{cs} from Eq. (6), this method searches for the height with maximum gradient (largest slope: $\mathrm{d}\sigma/\mathrm{d}h = \max.$). Since σ_{cs} obtained from contrast ratios is rather noisy this method leads to many inconsistent CBH values. To improve reliability, a Gaussian curve is first fitted to σ_{cs} and then the maximum gradient is sought for this smoothed profile (see Fig. 8).
- **CS MOR**: Using σ_{cs} from Eq. (6), this method searches for the height at which the meteorological optical range, given by equation

$$\mathrm{MOR} = -\frac{\ln(0.05)}{\sigma(h)} \approx \frac{3}{\sigma(h)} \tag{12}$$

  with a typical contrast ratio of 5 %, corresponds to a mandatory threshold value of $\mathrm{MOR}_{\mathrm{thr}} = 1000\,\mathrm{m}$. It represents the horizontal visibility and is already applied by some ceilometer manufacturers.
- **CS VOR**: Using σ_{cs} from Eq. (6), this method first calculates its vertical integral and then the height at which this vertical integral equals $-\ln(0.05) \approx 3$ is searched for. This height actually defines the vertical optical range, given by equation

$$\int_0^{\mathrm{VOR}} \sigma(h)\mathrm{d}h = 3 \tag{13}$$

  (see Chapter 6 in Weitkamp, 2005) assuming the recommended 5 % contrast ratio.
- **CS SOR**: Using σ_{cs} from Eq. (6), this method searches for the height at which the slant optical range, given by equation

$$\mathrm{SOR} = H\sqrt{\left(\frac{3}{\int_0^H \sigma(s)\mathrm{d}s}\right)^2 - 1} \tag{14}$$

  with a typical contrast ratio of 5 %, corresponds to a threshold value $\mathrm{SOR}_{\mathrm{thr}}$. For the latter, we tested values from 500 m to 1000 m with 100 m increment. From the geometric point of view SOR is the projection of an oblique line of sight onto the horizontal plane, which is shown by Fig. 4.
- **VS MOR**: Same as CS MOR but using σ_{vs} from Eq. (11) as extinction coefficient profile.
- **VS SOR**: Same as CS SOR but using σ_{vs} from Eq. (11) as extinction coefficient profile.

VOR is the limiting value of the SOR when looking vertically instead of obliquely. By definition, the VOR is always greater than the SOR, provided that the same contrast threshold is applied. All methods except RW CONT use $\sigma_{\mathrm{cs}}(h)$ or $\sigma_{\mathrm{vs}}(h)$ (see Sect. 3) as a basis for calculation. The CBH results obtained by the different, above-mentioned methods are compared with values provided by the ceilometer firmware in the next Sect. 5.

https://doi.org/10.5194/egusphere-2026-1696
Preprint. Discussion started: 19 May 2026

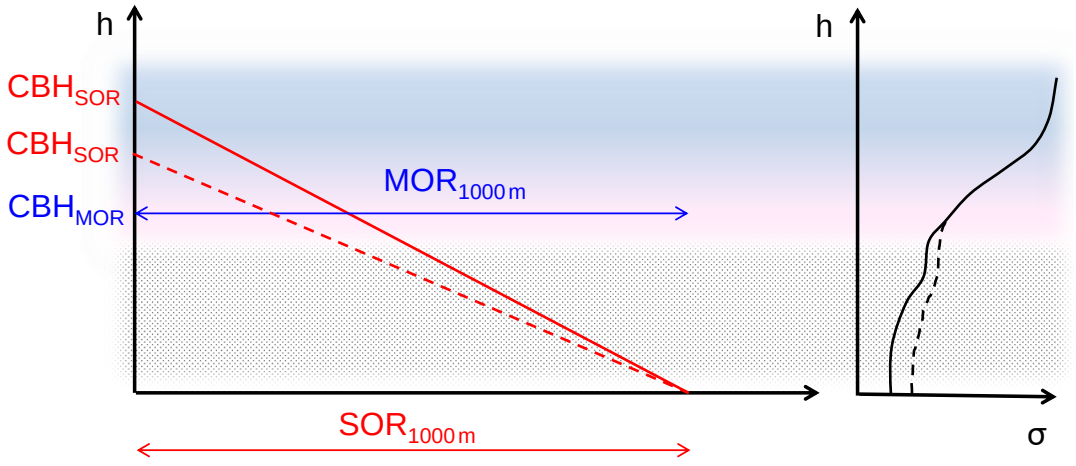

Figure 4. Schematic sketch of the MOR and SOR definition for the derivation of CBH. Only the SOR-based definition accounts for visibility conditions below the cloud, which inherently results in lower CBH values, since the extinction coefficient (σ) increases under conditions of reduced visibility.

When comparing Eq. (12) and Eq. (14), it becomes clear that only SOR considers the visibility below the cloud base through the integral of σ over height. Let's assume unrestricted visibility below cloud base and apply the same MOR threshold value of 1000 m also to SOR. In this case, the CBH calculated based on SOR is higher than the value calculated based on MOR (see Fig. 4). This behavior is absolutely realistic, as the cloud base is diffuse and for a pilot at final landing approach the visibility along the glide slope is relevant, not the horizontal visiblity at a certain flight altitude. If visibility deteriorates below the cloud base, the extinction coefficient increases in this height range. Consequently, the SOR-based CBH realistically decreases, while the MOR-based CBH remains unchanged. This underlines the superiority of the SOR over the MOR definition.

Figures 3(f−g) show the application of MOR and SOR definition to image analysis and complete the derivation of CBH on 04 November 2018 at 10:30 UTC. Here, image analysis using Eq. (6) and SOR definition yield a CBH value of 735 ft (CS SOR), compared to 623 ft (VS SOR) and 390 ft (VS MOR) when using Eq. (11) and either SOR or MOR definition.

5 Results

5.1 Comparison of analyzed methods

The CBH determination methods described in Sect. 4 were applied to data from the first phase of CircaHH, with six specific days examined in more detail: 12 and 25 November 2016, 31 December 2016, 22 January 2017 and 02−03 February 2017. These days were selected because the CBH comparison values provided by the ceilometers were sufficiently below the mast top and there was no snow on any of the mast platforms that would affect the performance when calculating the contrast ratios.

https://doi.org/10.5194/egusphere-2026-1696
Preprint. Discussion started: 19 May 2026

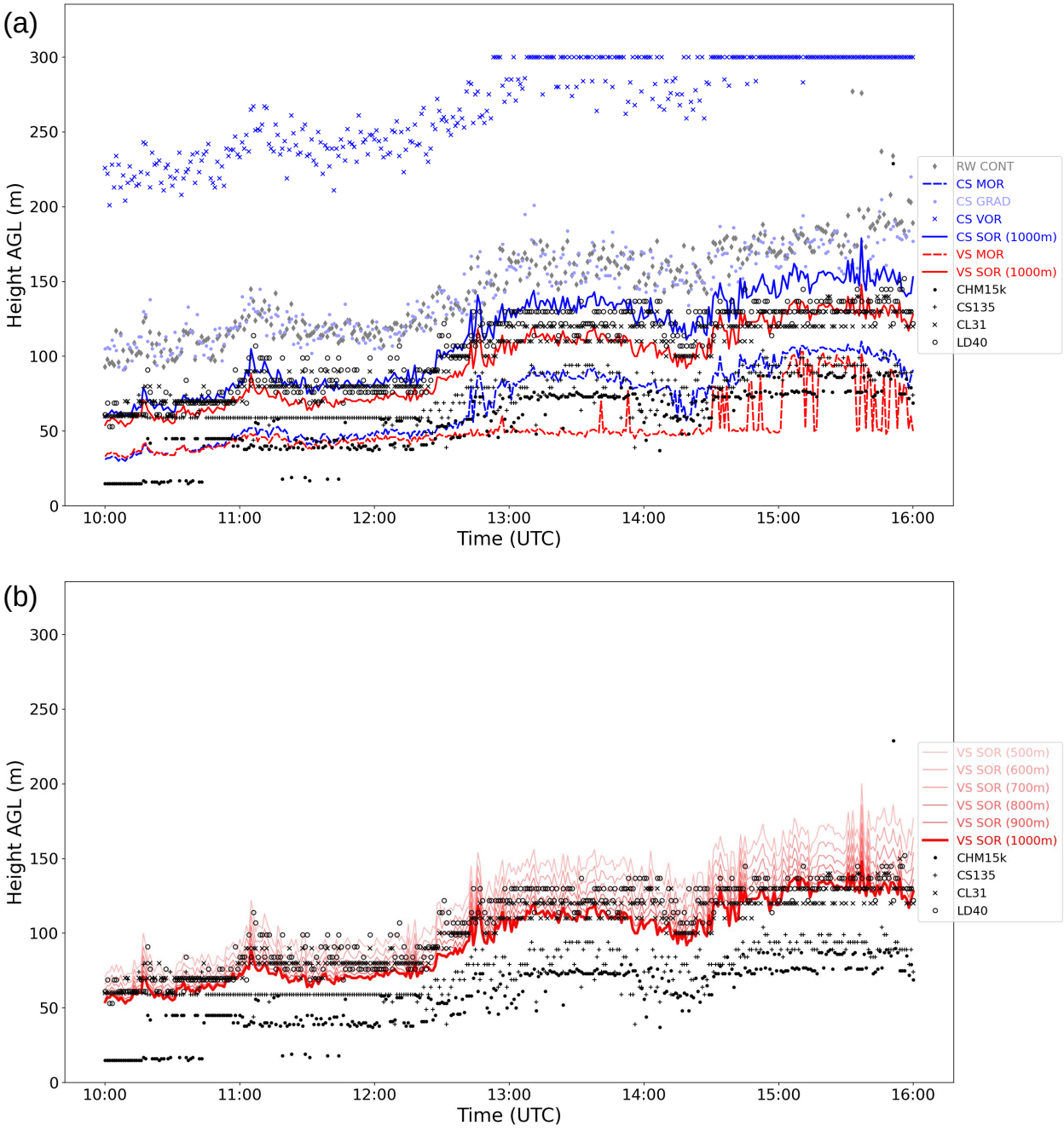

Figure 5. CBHs derived from **(a)** different methods according to Sect. 4 and from **(b)** SOR definition with different threshold values according to approach B) in Sect. 3 compared to CBH values determined by the ceilometers CHM15k, CS135, CL31 and LD40 on 03 February 2017 between 10:00 UTC and 16:00 UTC. The indices "CS" and "VS" mean "constant sigma" and "variable sigma" according to approach A) and B) in Sect. 3.

https://doi.org/10.5194/egusphere-2026-1696
Preprint. Discussion started: 19 May 2026

Figure 5(a) shows the results for 03 February 2017 using the abbreviations introduced in Sect. 4. CBHs determined by the ceilometers are represented by black symbols. This comparison confirms the systematic CBH differences (here up to 50 m) between ceilometers from different manufacturers mentioned in the introduction. The CS VOR method produces CBH values that are much higher (more than 100 m) than all other methods or ceilometer data. While the RW CONT and CS GRAD methods produce quite similar results, their CBHs are systematically higher than determined by all ceilometers. The remaining methods yield CBHs that are comparable to the values determined by the ceilometers. For example, the CS MOR method produces CBHs that are temporarily close to those of CS135 or CHM15k. As a side note but obvious in Fig. 5(a), the CBHs from CHM15k are sometimes (10:00−10:45 UTC) systematically too low. According to personal correspondence with OTT HydroMet, this behavior was first discussed by the Royal Netherlands Meteorological Institute (KNMI). This ultimately led to a change in the firmware, so that since version 0747, the *"higher low clouds"* option can be enabled, which systematically raises the CBHs derived from the CHM15k by 30−40 m up to 500 m height.

It is striking that both methods using the MOR definition (CS/VS MOR) produce almost identical CBHs until around 12:30 UTC, but then diverge significantly from each other, only to match again somewhat better from around 15:00 UTC onwards. The supplementary Fig. B1 helps to understand this behavior. As long as the σ_{cs}- and σ_{vs}-profiles are very similar within the lowest 100 m, both fall below MOR_{thr} in almost the same height level. If the extinction coefficient increases only slightly with height or even decreases, the σ_{vs} curve reaches MOR_{thr} earlier because it is shifted predominantly to higher values compared to σ_{cs}. According to Eq. (12) and starting from the ground, only the extinction coefficient at a certain height is checked for falling below the MOR threshold value, so that small differences in the extinction coefficient profile can cause large differences in the derived CBH.

Figure 5(b) illustrates the effect of different threshold values on the CBHs exemplarily for the SOR definition with variable extinction coefficient profile (VS SOR). Different shades of red are used to identify the six different SOR thresholds but the same labeling for the ceilometer data. The photo-derived CBHs are above and around the CBHs given by LD40 and CL31, with the CBH for the 1000 m threshold being closest to the ceilometer CBH. CBHs derived from the VS SOR method are even closer to the ceilometer results than for the CS SOR method and agree very well with those of the LD40 and CL31.

Let's keep these interim results in mind and move on to the more recent measurements from the third CircaHH phase, in particular from 04 November 2018 between 09:00 UTC and 12:00 UTC (Fig. 6). The photo sequence in Fig. 6(a) suggests a cloud layer with increasing CBH approximately between 150 m and 300 m height. According to Fig. 6(c), there is no precipitation over these three hours. MOR is always higher than 4 km (nearly unrestricted horizontal visibility) at 2 m height, mostly lower than 100 m (strongly restricted horizontal visibility) at 280 m height and increases from less than 100 m to more than 2 km at 175 m height.

https://doi.org/10.5194/egusphere-2026-1696
Preprint. Discussion started: 19 May 2026

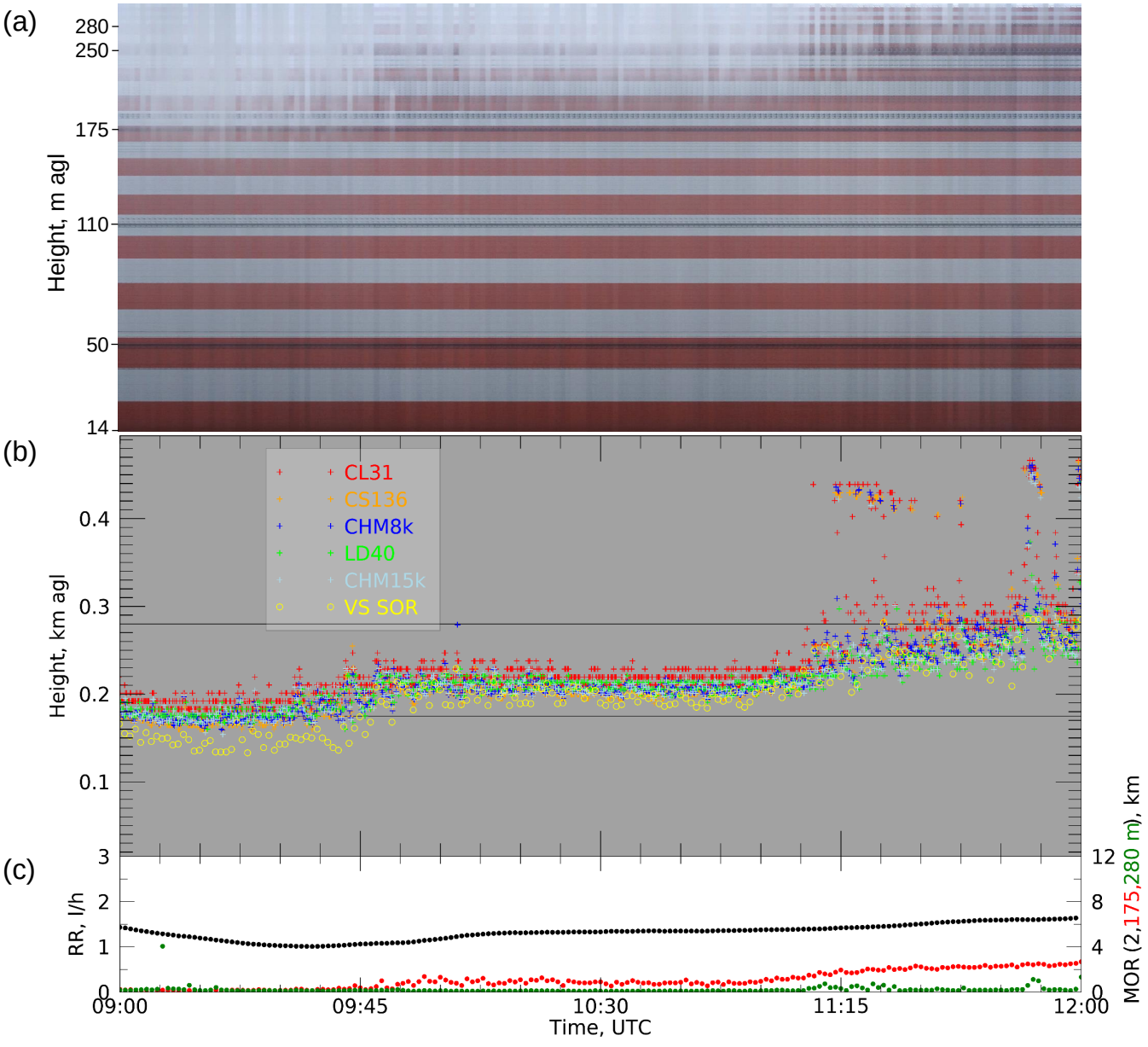

Figure 6. **(a)** Sequence of 1 min cropped photos from the Hamburg Weather Mast; **(b)** CBHs derived by the VS SOR method according to Sect. 4 compared to ceilometer values of CL31, CS136, CHM8k, LD40 and CHM15k; **(c)** Precipitation rate (RR) and MOR in three different heights all shown for 04 November 2018 between 09:00 UTC and 12:00 UTC. No blue bars mean it did not rain. The two black horizontal lines represent the PWD20 in 175 m and 280 m and the PWS100 is used analogously to get the value of MOR in 2 m height.

Figure 6(b) confirms that the above-mentioned firmware change results in higher CBHs from CHM15k. Compared to Fig. 5(a) the CBHs from CL31, CS136 and CHM8k better match the results of LD40. This is explained by a corresponding requirement

https://doi.org/10.5194/egusphere-2026-1696
Preprint. Discussion started: 19 May 2026

of the DWD in the specifications within the framework of the international tender for the replacement of the LD40 at Germany's 15 international airports. However, Fig. 6(b) shows that the CBH differences between the manufacturer-specific ceilometer algorithms and in comparison to the image analysis (VS SOR, *yellow circles*) are up to several 100 m. At 10:30 UTC, for example, the maximum CBH difference between ceilometers and image analysis is only about 30 m, while at 09:44 UTC it is about 90 m and at 11:15 UTC even about 230 m. The VS SOR method, which applies the SOR definition to σ_{vs} (Sect. 4), results in lower CBH values, in particular from 09:00 UTC to 09:45 UTC, when visibility below the cloud is restricted. This is consistent with the theoretical considerations in Sect. 3 based on Fig. 4. The saturation behavior of CBHs from VS SOR, i.e. 285 m at most between 11:50 UTC and 11:52 UTC, in Fig. 6(b) results from the fact that the image analysis is limited vertically to the usuable mast segment pairs and the mast size in general.

All individual steps for determining the CBH based on image analysis are already shown in Fig. 3, with the focus on 10:30 UTC on 04 November 2018. Figure 3(f) shows that the CBH from VS SOR is lower than from CS SOR and that the CBH for the MOR definition (VS MOR) is generally lower than the SOR-based values. Are the extinction coefficients derived from the image analysis at all plausible and of sufficient quality?

5.2 Quality assessment of image analysis

Figure 6 demonstrates that the CBHs determined by image analysis are plausible and realistic. First, the development of CBHs over time corresponds to that of ceilometers (Fig. 6(b)). Second, the MOR values at 2 m, 175 m and 280 m (Fig. 6(c)) agree qualitatively with the general temporally increasing CBH. Third, the SOR definition (*yellow cirlcles*) even provides more realistic CBH values for "poorer" (09:00−09:45 UTC) and "better" (11:15−12:00 UTC) visibility conditions below the cloud layer. In poor visibility conditions Fig. 6(c) clearly shows that the MOR for both PWD20 sensors has comparable values of around 100 m, indicating that the CBH should be lower than 175 m. With improved visibility, the MOR of the PWD20 at 175 m is significantly greater than that at 280 m, so that the CBH should be somewhere in between or slightly above 280 m. This expected behavior is only partially met by the ceilometers. However, from around 11:15 UTC, the cloud layer is obviously more inhomogeneous, which leads to a greater scattering of CBHs.

For a more quantitative assessment the two *green squares* in Fig. 3(e) show the extinction coefficients derived from the MOR measurement of the PWD20 sensors in 175 m and 280 m height, respectively. In the vast majority of cases, these *green squares* correspond much better with the σ_{vs} curve (*red solid line*) representing the variable extinction coefficient profile according to Eq. (11). Furthermore, the corresponding *green squares* in Fig. 3(g) tend to agree best with the VS MOR curve (*blue solid line*) that is the vertical visibility profile derived from the MOR definition applied to σ_{vs}. The supplementary Figs. B2 to B5, analogous to Fig. 3, confirm these statements for further points in time. This means, on the one hand, that σ_{vs} derived from image analysis best reflects the actual extinction coefficient profile and, on the other hand, that when using the MOR definition instead of CBH, only the horizontal visibility at a certain height is determined.

Figure 7 shows the comparison of the extinction coefficient between image analysis (σ_{vs}) and derived from visibility measurements of the PWD20 sensors in 175 m and 280 m height for the same time period as in Fig. 6. The good agreement of the extinction coefficient at least at 175 m confirms the applicability of our image analysis to determine σ. The slightly larger

https://doi.org/10.5194/egusphere-2026-1696
Preprint. Discussion started: 19 May 2026

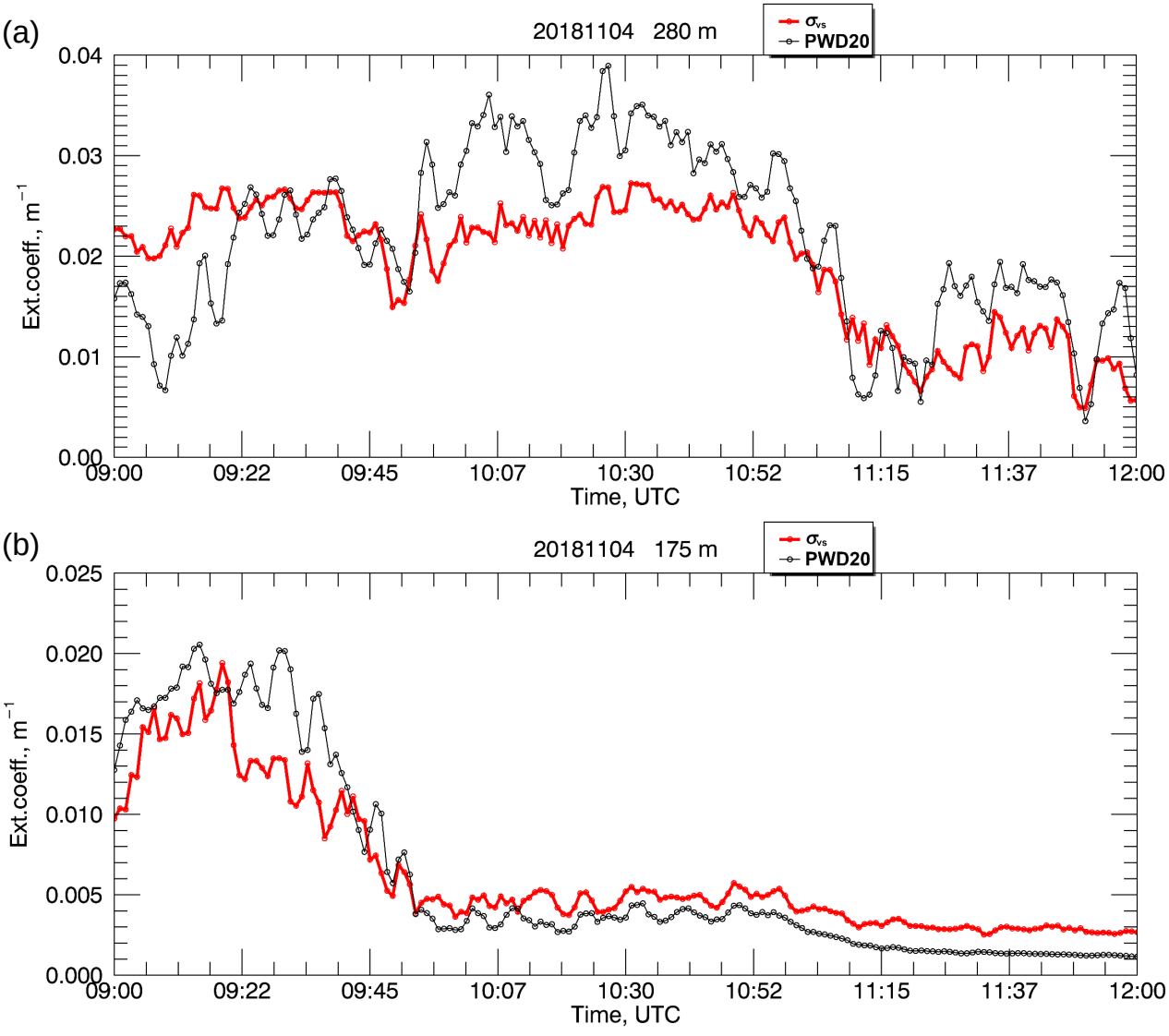

Figure 7. Extinction coefficient $\sigma_{vs}(h)$ in m^{-1} derived from image analysis using Eq. (11) in Sect. 3 and visibility measurements of the PWD20 in **(a)** $h = 280\,\mathrm{m}$ and **(b)** $h = 175\,\mathrm{m}$ height on 04 November 2018 between 09:00 UTC and 12:00 UTC.

deviations at 280 m can be attributed to sensor problems. A quantitative comparison of the extinction coefficient with the PWS100 at a height of 2 m is not possible, as image analysis only begins at a height of approximately 14 m and we can assume horizontal but not vertical homogeneity.

https://doi.org/10.5194/egusphere-2026-1696
Preprint. Discussion started: 19 May 2026

5.3 Error estimation of image analysis

As mentioned in the introduction (Sect. 1), there is currently neither a reference method nor a reference device that could be used to quantitatively determine the quality of the derived extinction coefficient profile for very low clouds. Given the sometimes large variation in CBH values from different manufacturers for the same cloud situation (e.g. Fig. 5 and Fig. 6), the CBH determined with a ceilometer or even the average value of all ceilometers considered cannot be reliably used as a reference value, for example, to calculate the root mean square error. Therefore, we are unfortunately unable to provide an absolute or relative error value here.

To estimate the error or rather uncertainty of our image analysis method (Sect. 3), we generally consider "optimal conditions": i) stable cloud layer without gaps; ii) CBH significantly less than 300 m; iii) no precipitation (neither rain nor snow fall); iv) no ground fog. However, there is a distinction between good and poor visibility below the cloud base. Figure 8 shows typical average results for a 20-minute period. For most of the methods described in Sect. 4, both the underlying extinction coefficient profile and the derived CBH mean value and variance are shown here with corresponding color coding. The mean value and variance derived from the ceilometer CBHs are also shown in Fig. 8. In contrast, the values for the VS MOR method are not specified, as the use of the σ_{vs}-profile leads to unrealistic jumps in the CBH (see Fig. 5(a)). These CBH jumps occur although the σ_{cs}-profile differs rather slightly (supplementary Fig. B1) and therefore, the MOR definition is generally too sensitive and not robust enough.

While the VS SOR method produces CBH values that are lower than those of ceilometers or lie in the middle of their value range when visibility is restricted (Fig. 8(b)), it generally shows higher CBH values when visibility is good below the cloud base (Fig. 8(a)). Good or poor visibility is well reflected by the respective extinction coefficient profiles and the derived CBH agrees with the theoretical considerations in Sect. 3 based on Fig. 4. Particularly in poor visibility conditions, the VS SOR method provides the lowest uncertainty in the CBHs derived from image analysis, and this uncertainty is even lower than with all ceilometers.

https://doi.org/10.5194/egusphere-2026-1696
Preprint. Discussion started: 19 May 2026

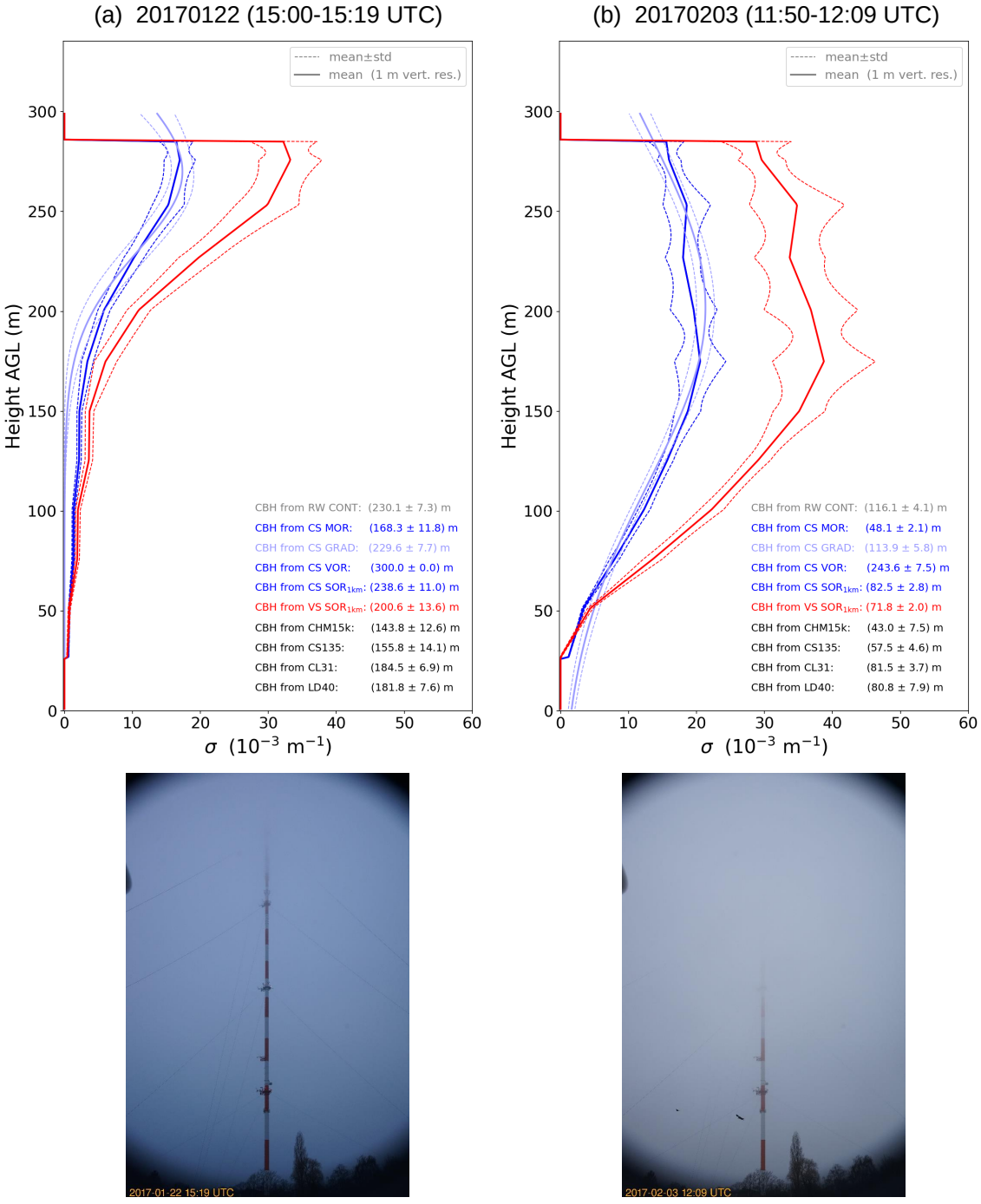

Figure 8. 20 min mean vertical profile of the extinction coefficient and its standard deviation (vertical resolution of 1 m), determined from image analysis using σ_{cs} (*blue*) from Eq. (6) and σ_{vs} (*red*) from Eq. (11) for two time periods with stable cloud layer. The lightblue extinction coefficient profile is the required Gaussian fit for the CS GRAD method. The respective CBH values are given, which are derived from the methods in Sect. 4 or supplied by the ceilometer firmware. The mast photos below were taken with Sony $\alpha 7$ at the end of the respective 20 min period.

https://doi.org/10.5194/egusphere-2026-1696
Preprint. Discussion started: 19 May 2026

5.4 Insights from Klett inversion method

An obvious cross-check for the SOR definition with a threshold of 1000 m is its application to the extinction coefficient profile derived from ceilometer data. For this purpose, we use our own implementation of the Klett inversion method (KIM) described in Appendix A. It is not directly applicable to operational use, but certainly provides insight into the credibility and applicability of the SOR definition for determining CBH. In particular, we use β_{att} from CL31, CS136 and CHM8k collected during the international tender 2018/19 to replace the LD40 airport ceilometers at German international airports (see Sect. 2). While CBH values in the reprocessed data are in a sense tuned to LD40, as it was used as the reference device to determine probability of detection and false alarm rate, the originally provided β_{att} remained unchanged from the respective firmware adjustments.

Figure 9 shows that, regardless of the ceilometer input data, the CBHs derived using the KIM better reflect the temporal structure of β_{att} than the CBHs from the proprietary ceilometer algorithms. Interestingly, the KIM provides CBHs that tend to appear above the β_{att} peak. The curves for $\mathrm{KIM_{CL31}}$ and $\mathrm{KIM_{CHM8k}}$ are very similar, even though the latter shows slightly lower CBHs. In contrast, $\mathrm{KIM_{CS136}}$ is systematically shifted upwards with some significantly higher CBHs. This is completely the opposite for the manufacturer algorithms and the CBHs determined by the CS136 firmware are systematically lower than those determined by the CHM8k firmware. It is evident that the differences between the CBH values determined using the KIM for the various ceilometer input data are significantly smaller than the CBH differences associated with different ceilometer algorithms. As confirmation, we provide the mean value and standard deviation of CBH for the plateau range from 10 UTC to 11 UTC in Fig. 9: 210.2 ± 3.4 m for LD40, 207.4 ± 4.8 m for CHM15k, 205.2 ± 5.7 m for CL31, 192.8 ± 3.5 m for CS136, 207.0 ± 4.3 m for CHM8k, 223.4 ± 5.4 m for $\mathrm{KIM_{CL31}}$, 231.0 ± 5.6 m for $\mathrm{KIM_{CS136}}$ and 220.0 ± 5.4 m for $\mathrm{KIM_{CHM8k}}$. The variance of the CBH values from the KIM is of the same order of magnitude as that of the ceilometers and agrees best with the CL31 here. Between 11:14 UTC to 11:25 UTC, only the KIM using the SOR definition is capable of deriving CBHs that correspond to the temporal structures of β_{att}. The gaps or optically thinner sequences in the lower cloud layer lead to the CBHs between 1250 ft and 1500 ft height, which is not captured by the ceilometer algorithms.

Figure 10 shows the original β_{att}-profiles of CL31, CS136 and CHM8k on 04 November 2018 at 10:30 UTC, whereby the peak generally appears below 1000 ft AGL and has the largest magnitude for CS136. Although CHM8k produces the smallest peak magnitude it shows the smallest noise in the upper height levels. Noise reduction of KIM effectively removes β_{att} values above approximately 1000 ft here, while both the height and the magnitude of the peak remains unchainged. The respective σ-profile and final CBH derived from KIM using the SOR definition with a threshold value of 1000 m are also shown in Fig. 10. While the σ-profiles from CS136 and CHM8k input data are qualitatively very similar and agree fairly well with the result from image analysis (Fig. 3(e)), the σ-profile obtained from CL31 input data has at least an unusual shape above 800 ft height. According to the *horizontal green lines* in Fig. 10, the CBHs are 722 ft for CL31, 755 ft for CS136 and 688 ft for CHM8k input. The differences between these values and the value derived from image analysis (last paragraph in Sect. 4) for CS SOR are: -13 ft (CL31), $+20$ ft (CS136), -47 ft (CHM8k), while the differences relative to VS SOR are: $+99$ ft (CL31), $+132$ ft (CS136), $+65$ ft (CHM8k). Overall, the differences compared to image analysis with CS SOR are smaller.

So far, we mainly investigated very low clouds under optimal conditions as defined in Sect. 5.3, for which the CBH must

https://doi.org/10.5194/egusphere-2026-1696
Preprint. Discussion started: 19 May 2026

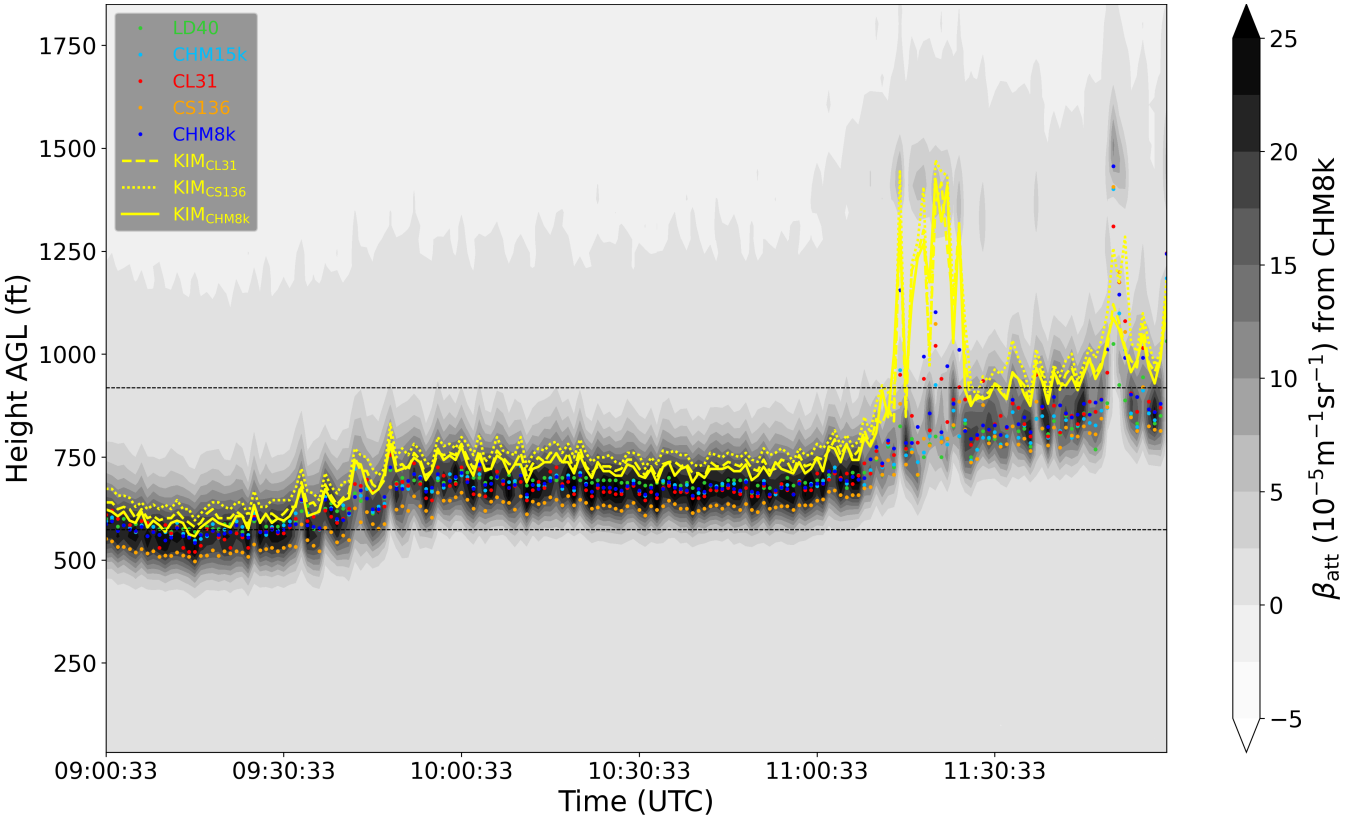

Figure 9. Minute mean values of attenuated backscatter (β_{att}) from CHM8k, CBHs derived from manufacturer algorithms for LD40, CHM15k, CL31, CS136, CHM8k and derived from the Klett inversion method (KIM) together with the SOR definition (Eq. (14)) using a threshold value of 1000 m and β_{att} input from CL31, CS136 or CHM8k (*subscript*) for the same time period as in Fig. 6.

be reliably derived in any case. As also mentioned in Appendix A our KIM implementation needs further improvement and tuning before being put into operational use. On the one hand, the algorithm could be expanded to identify more than just the lowest cloud layer, although this is the most relevant for aviation. Linear interpolation of the σ-profile could increase the current vertical resolution from 10 m to, for example, 1 m, which in turn would probably result in slightly lower CBHs. On the other hand, the performance of the SOR definition still needs to be analyzed in detail for clouds with precipitation or fog and over a longer period of time. This is ongoing work and beyond the scope of this study, as the focus here is on the formulation of a suitable quantitative definition of CBH.

https://doi.org/10.5194/egusphere-2026-1696
Preprint. Discussion started: 19 May 2026

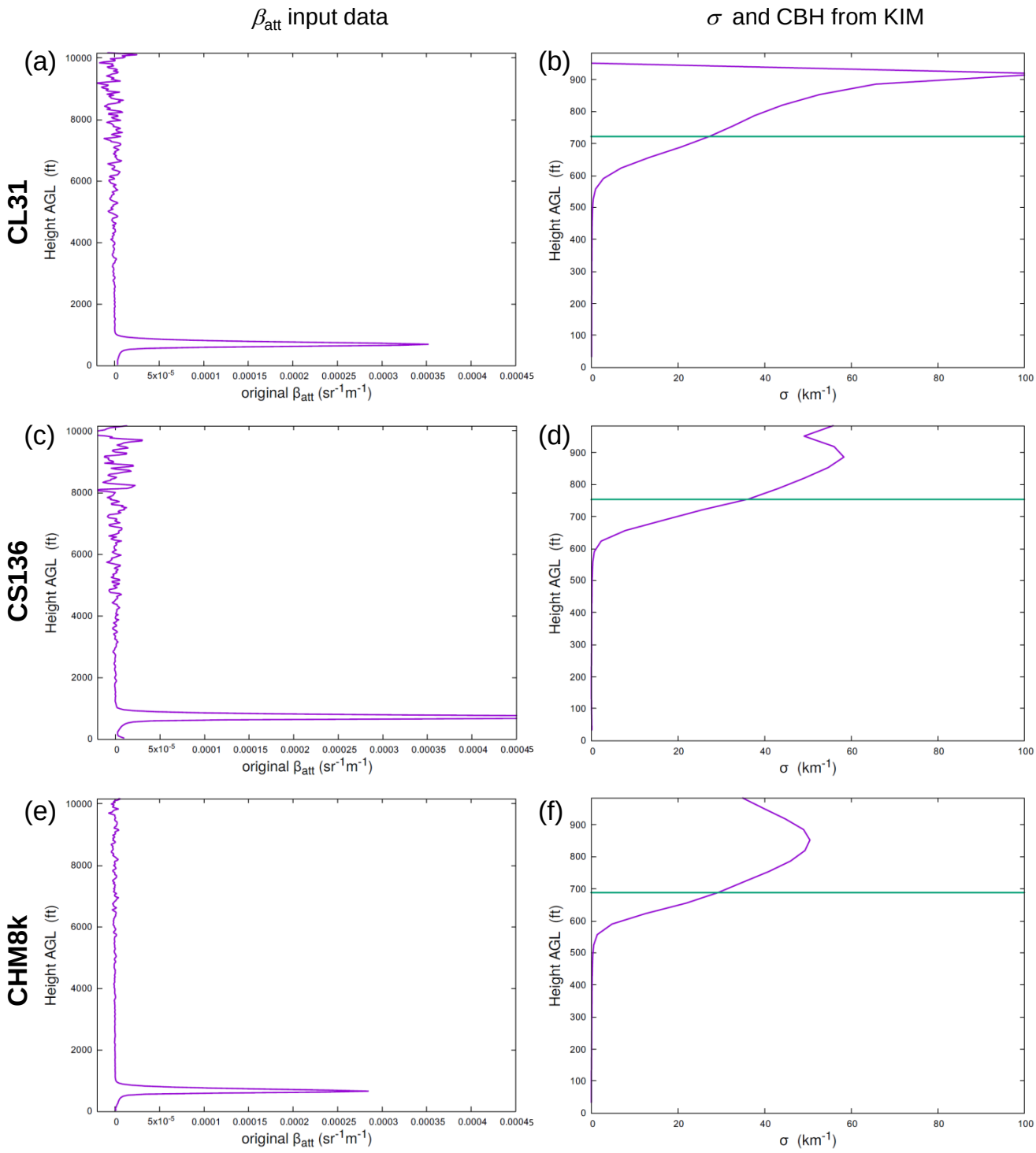

Figure 10. Original β_{att}-profile measured by **(a)** CL31, **(c)** CS136, **(e)** CHM8k on 04 November 2018 at 10:30 UTC and **(b), (d), (f)** the respective vertical profile of the extinction coefficient (σ) as well as the CBH (*horizontal line*) derived from the Klett inversion method (KIM) using the SOR definition with a threshold value of 1000 m.

https://doi.org/10.5194/egusphere-2026-1696
Preprint. Discussion started: 19 May 2026

6 Conclusions

The CBH measured by various ceilometers differ significantly due to differences in the actually measured backscatter signal and the lack of a universally accepted definition of the cloud base. Particularly in situations with very low clouds, the question arises as to which CBH meets the requirements of aviation. Therefore, a number of methods were tested for their ability and effectiveness to derive CBH mostly from the extinction coefficient profile obtained by image analysis of photos from a 300 m tall mast. In the model study by Lewis et al. (2022), efforts have already been made to derive CBH using artificial intelligence, but this is not applicable to our image analysis for determining the σ-profile.

There are suitable CBH criteria based on image analysis, which can basically reproduce the CBH from ceilometers. The contrast ratio method (RW CONT) and the maximum gradient method (CS GRAD) tendentially result in CBHs that are in the upper range or just above those of the CL31 and especially the LD40. In contrast, the horizontal visibility method (CS/VS MOR) with the known threshold of $\mathrm{MOR_{thr}} = 1000\,\mathrm{m}$ usually provides CBHs that match those of the CS135 and CS136. Although used by some ceilometer manufacturers (e.g. Campbell, 2018, Appendix C), the MOR definition has the major disadvantage that it cannot take into account visibility conditions below the cloud and it is very sensitive to the underlying extinction coefficient profile, meaning that small vertical changes in σ can cause large differences in the derived CBH including artificial jumps.

The extinction coefficient integral method (CS VOR) yield CBHs that are systematically too high. This is consistent with the model study by Stoelinga and Warner (1999) and confirms the statement of Gaumet et al. (1998) that vertical visibility as defined by Eq. (13) is not the most suitable quantity for final landing approach. Otherwise, the application of a threshold value lower than 3 in Eq. (13) is conceivable as a CBH definition, but it should then no longer be referred to as VOR. In general, the CBH values determined with the ceilometers are well reproduced by the SOR method, whereby the CBH is systematically lower as the threshold value increases. Using $\mathrm{SOR_{thr}} = \mathrm{MOR_{thr}}$ the CBHs are in best agreement with LD40, CL31 and CHM15k and the variable extinction coefficient profile (VS SOR) gives the most realistic results for image analysis. A real-world example that can be compared to the SOR method comes from Eberhard (1986), where the CBH was determined by a pilot determining when the ground was no longer visible.

On the basis of measurements carried out during three phases of CircaHH our unique results suggest that: i) Our image analysis can provide a reference method to evaluate β_{att} obtained from any ceilometer and it can serve as quality check for CBHs derived by the ceilometer firmware; ii) The SOR derived according to Eq. (14) with a threshold value of 1000 m appears to be a suitable and robust quantitative CBH definition as visibility conditions between the ground and the cloud base are taken into account; iii) This SOR definition is especially valuable for aviation, providing pilots with more useful information for an oblique downward or upward view.

Our implementation of the Klett inversion method confirms the applicability and added value of the above-mentioned SOR definition for low clouds. It is noteworthy that the independent derivation of the σ-profile via image analysis or KIM ultimately leads to very similar CBHs. Therefore, our KIM with SOR definition offers a physically motivated method to derive CBH on the basis of the ceilometer backscatter signal and has the potential to improve the automated determination of airport weather

https://doi.org/10.5194/egusphere-2026-1696
Preprint. Discussion started: 19 May 2026

reports like METAR and MET REPORT. However, our KIM implementation still needs further improvement before it can be put into operational use.

Code availability. Both the IDL source code for our image analysis and the C^{++} source code for our KIM implementation are provided as supplementary material under the condition "access limited to reviewers". Since especially the KIM implementation still needs to be further improved and optimized, and a detailed description is planned in a separate article, it can only be made available on a confidential basis.

Data availability. The image and measurement data underlying this publication have been uploaded to Zenodo (Klaus and Görsdorf, 2026) and are freely available. Additional CircaHH data can be provided by the corresponding author upon request. However, the total storage requirement for the entire dataset is enormous, particularly because of the image files.

Appendix A: Implementation of Klett inversion

To calculate the extinction coefficient profile from the backscatter signal measured by the ceilometer, we use the backward inversion method originally described by Klett (1981), but in accordance with Ferguson and Stephens (1983) and with the improvements suggested by Mulders (1984). Our modular C^{++} source code is still not directly applicable to operational use. Since we started with LD40 input data and we only know all the necessary parameters for this ceilometer, for example for calculating the constant C_1 from Ferguson and Stephens (1983), we generally use a few LD40 parameters as a test environment for each ceilometer. The key steps in our implementation are as follows:

1. For the constant C_1 in Eq. (2) of Ferguson and Stephens (1983) we take over $1\,\mu\mathrm{J\,m^{-2}}$ as transmitted power per pulse and $50\,\mathrm{ns}$ as laser pulse duration both from de Haij et al. (2006) and we use $140\,\mathrm{mm}$ as diameter from the LD40 manual (Vaisala, 2005) to obtain the effective area of the receiver objective.

2. We follow Eq. (3) of Ferguson and Stephens (1983), set the constant C_2 to $0.05\,\mathrm{sr^{-1}}$ and the exponent of the power law to $k = 1$, which are the most frequently cited values for liquid water clouds as discussed by Gaumet et al. (1998). This corresponds to a particle lidar ratio of $20\,\mathrm{sr}$, which agrees quite well with the experimentally determined values summarized in Table 3 by ISO 28902-4 (2025) from more recent studies. Both the extinction coefficient and backscatter coefficient are assumed to be constant along the optical path.

3. Depending on the ceilometer the current implementation reads the range-corrected backscatter coefficient (β_{rc}) or the attenuated backscatter coefficient (β_{att}) from daily NetCDF files. Both backscatter values are usually already background corrected. Here we focus on the reprocessed data from CL31, CS136 and CHM8k that means ideally 8640 records of β_{att} are respectively available for $10\,\mathrm{s}$ report time interval with vertical resolution of $9.99\,\mathrm{m}$ from $9.99\ \mathrm{m}$ to $7692.3\ \mathrm{m}$ height (770 levels).

https://doi.org/10.5194/egusphere-2026-1696
Preprint. Discussion started: 19 May 2026

4. Necessary noise reduction and averaging are applied to the original backscatter signal according to Sect. 3.1 of van Tricht et al. (2014). Noisy data is removed if the signal-to-noise ratio (SNR) is higher than 1, which is checked for every separate vertical level. Just like van Tricht et al. (2014), we use 20 profiles before and after the current time ($M = 20$). In contrast, we have 6 profiles per minute instead of 4 and therefore our averaging is only done over $\pm 3\,\mathrm{min}\ 20\,\mathrm{s}$ instead of $\pm 5\,\mathrm{min}$ resulting in less smoothing.

5. Calculation of $\sigma(r_\mathrm{f})$ using Eqs. (6) to (8) by Mulders (1984) instead of the iteration steps (2) to (4) by Ferguson and Stephens (1983):

   - calculation of $S_\mathrm{m}(r)$ with Eq. (1) of Mulders (1984)
   - determination of S_0 with index r_0, where the absolute value of S_m is higher than zero (and unequal NaN) for the first time starting at the lowest level
   - calculation of $\sigma(r_0)$ with Eq. (8) of Mulders (1984)
   - identification of the far end index r_f, where the absolute value of S_m is higher than zero (and unequal NaN) for the first time starting at the level index that corresponds to about 10,000 ft AGL (does not work for multiple cloud layers)
   - equating Eq. (6) of Mulders (1984) to zero and rearranging gives the fix-point-form equation

     $$\sigma(r_\mathrm{f}) = \left[e^{(S_0 - S_\mathrm{m}(r_\mathrm{f}))/k} - 2 \cdot I/k\right]^{-1}. \tag{A1}$$

     The first term in square brackets on the right-hand side can easily be calculated as all contributions are known. The second term can be determined by numerical integration of Eq. (7) of Mulders (1984) currently using the rectangular rule for the scalar (fixed point) iteration.

6. Iterative calculation of $\sigma(r)$ using Eq. (9b) of Ferguson and Stephens (1983) to obtain the entire vertical profile from r_0 to r_f.

7. Successive calculation of SOR using Eq. (14), whereby SOR decreases with increasing height, and application of $\mathrm{SOR_{thr}} = 1000\,\mathrm{m}$ to determine the CBH of the first cloud layer ($\mathrm{CBH_1}$) starting from the lowest level. The vertical resolution of the final $\mathrm{CBH_1}$ is currently restricted to the discrete height levels of the input backscatter data (here $10\,\mathrm{m}$).

To get accurate vertical profiles, for example of S_m, we use a linear extrapolation to replace NaN values from level index r_0 to 0 and a linear interpolation to replace NaN values between r_0 and r_f. The latter is only performed if the respective gap in the profile is less than $100\,\mathrm{m}$; otherwise, the NaN values remain unchanged. The effect of, for example, a modified SNR threshold or another value for M on the CBH results will be investigated in the future. Once our Klett inversion method is selectively improved, tuned and sufficiently reliable for operational use, we will present it in detail in a separate publication.

https://doi.org/10.5194/egusphere-2026-1696
Preprint. Discussion started: 19 May 2026

Appendix B: Supplementary results

The following pages show the supplementary Figs. B1 to B5 that clarify and/or confirm already shown results and conclusions.

https://doi.org/10.5194/egusphere-2026-1696
Preprint. Discussion started: 19 May 2026

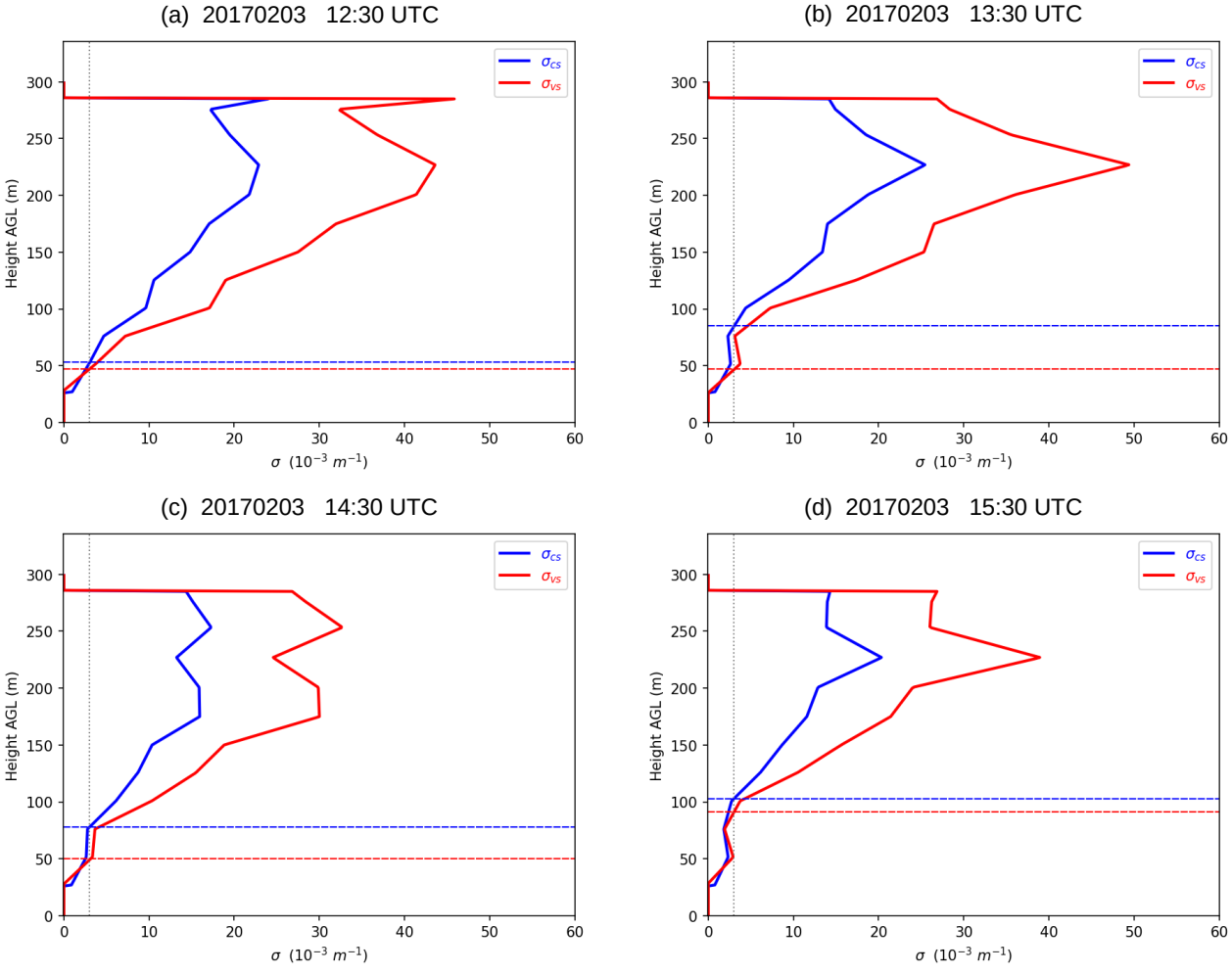

Figure B1. Vertical profiles of σ_{cs} from Eq. (6) and σ_{vs} from Eq. (11) with their CBHs (*horizontal line*) derived from the MOR definition according to CS MOR and VS MOR in Sect. 4 for four timestamps on 03 February 2017. The vertical grey dotted line marks the extinction coefficient of $3 \cdot 10^{-3}\,\mathrm{m}^{-1}$ that corresponds to the threshold value $\mathrm{MOR}_{\mathrm{thr}} = 1000\,\mathrm{m}$. These supplementary results help to understand the sometimes large differences in Fig. 5(a).

https://doi.org/10.5194/egusphere-2026-1696
Preprint. Discussion started: 19 May 2026

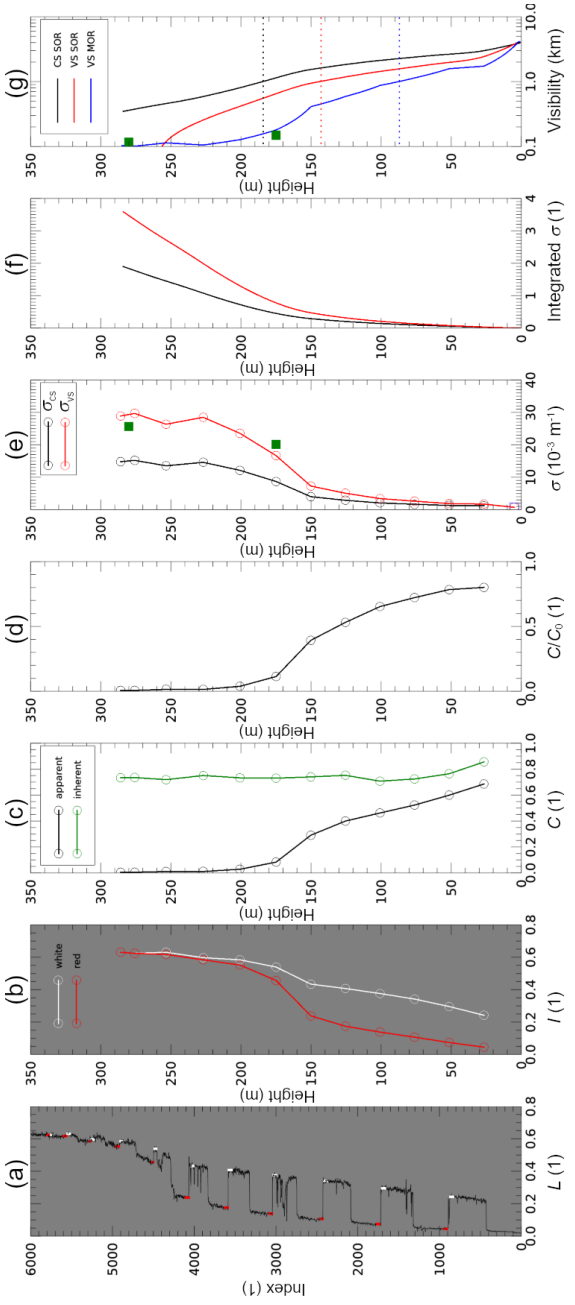

Figure B2. Same as Fig. 3 but for 04 November 2018 at 09:30 UTC.

https://doi.org/10.5194/egusphere-2026-1696
Preprint. Discussion started: 19 May 2026

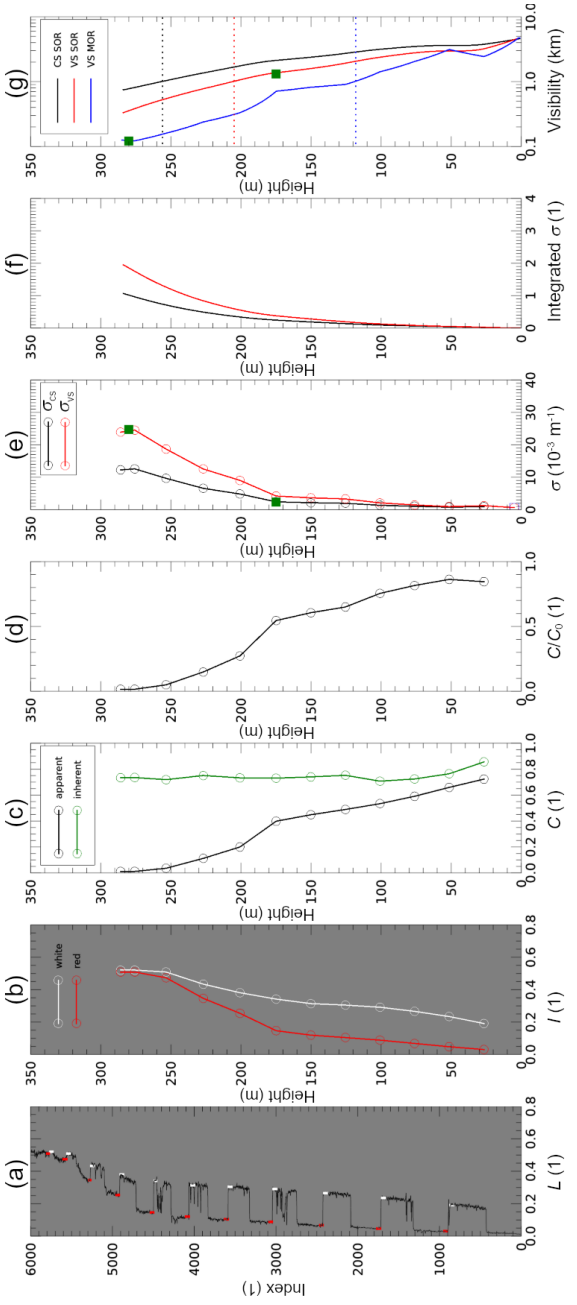

Figure B3. Same as Fig. 3 but for 04 November 2018 at 10:00 UTC.

https://doi.org/10.5194/egusphere-2026-1696
Preprint. Discussion started: 19 May 2026

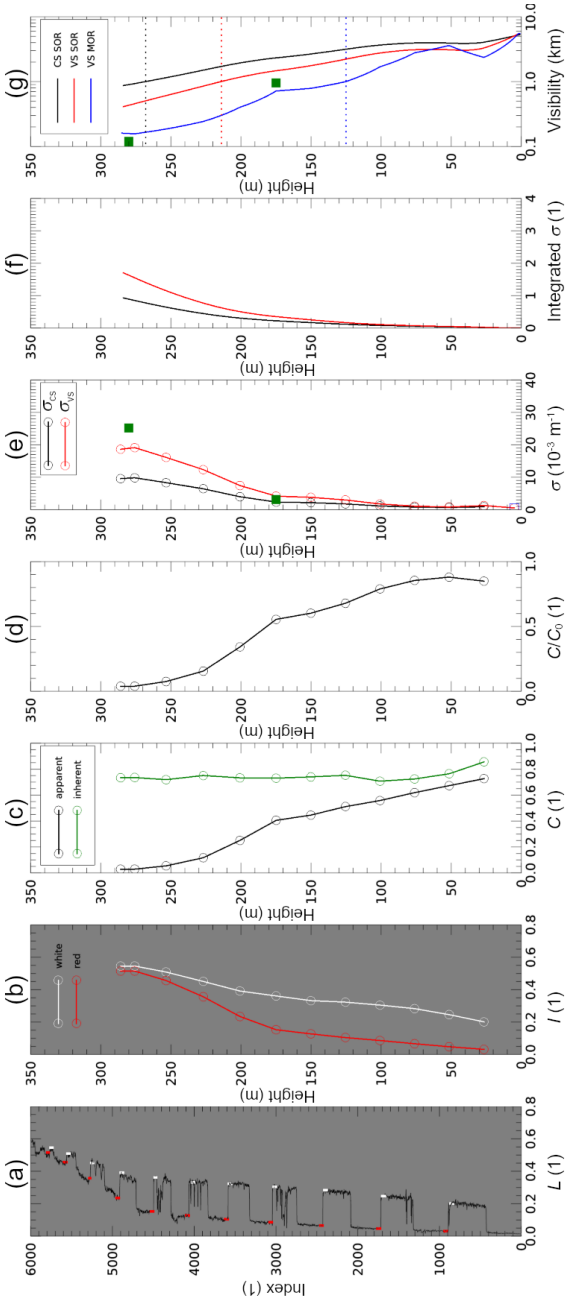

Figure B4. Same as Fig. 3 but for 04 November 2018 at 11:00 UTC.

https://doi.org/10.5194/egusphere-2026-1696
Preprint. Discussion started: 19 May 2026

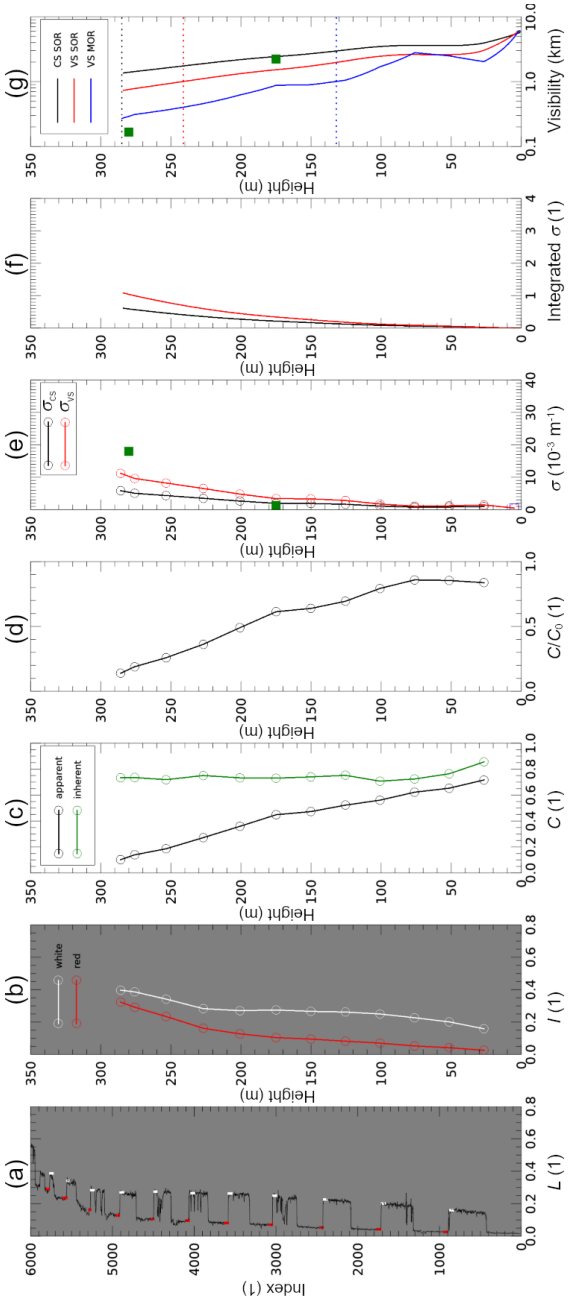

Figure B5. Same as Fig. 3 but for 04 November 2018 at 11:30 UTC.

https://doi.org/10.5194/egusphere-2026-1696
Preprint. Discussion started: 19 May 2026

Author contributions. UG contributed to the conceptualization of this study. JZ developed the fundamentals for our image analysis; UG and DK performed the measurements; DK, UG, and RD analyzed the data; DK implemented the Klett inversion method and wrote the manuscript draft; DK, UG, RV, JV, and JZ reviewed and edited the manuscript.

Competing interests. The authors declare that they have no conflict of interest.

Acknowledgements. This study was carried out with the financial, logistical and technical support of Deutscher Wetterdienst (DWD). The authors would like to express their sincere thanks to the ceilometer manufacturers OTT HydroMet, Vaisala, and Campbell Scientific for consenting to the publication of the data from the international tender (09/2018−01/2019). Special thanks go to the German television station "Norddeutscher Rundfunk" (NDR) for the permission and support of measurements during the CircaHH campaigns. We would like to thank the Meteorological Institute of University of Hamburg, especially Ingo Lange, for the excellent cooperation, for provision of the infrastructure, the delivery of the data from the "Hamburg Weather Mast", and the support of our systems (PWD20 data recording, ceilometer maintenance work). We also thank Patrick Laufing, Sven Voland and Ronny Leinweber for the installation of the measuring instruments and technical support.

https://doi.org/10.5194/egusphere-2026-1696
Preprint. Discussion started: 19 May 2026

References

Althausen, D., Engelmann, R., Baars, H., Heese, B., Ansmann, A., Müller, D., and Komppula, M.: Portable Raman Lidar Polly^{XT} for Automated Profiling of Aerosol Backscatter, Extinction, and Depolarization, J. Atmos. Oceanic Technol., 26, 2366–2378, https://doi.org/10.1175/2009JTECHA1304.1, 2009.

Campbell: USER GUIDE CS135 Ceilometer, Campbell Scientific Ltd, 80 Hathern Road, Shepshed, Loughborough, UK, User Manual, 92 pp., 2014.

Campbell: INSTRUCTION MANUAL PWS100 Present Weather Sensor, Campbell Scientific Ltd, 80 Hathern Road, Shepshed, Loughborough, UK, User Manual, Revision: 11/15, 122 pp., 2015.

Campbell: INSTRUCTION MANUAL CS120A and CS125 Visibility and Present Weather Sensors, Campbell Scientific Ltd, 80 Hathern Road, Shepshed, Loughborough, UK, User Manual, Revision: 6/16, 88 pp., 2016.

Campbell: INSTRUCTION MANUAL CS136 Ceilometer, Campbell Scientific Ltd, 80 Hathern Road, Shepshed, Loughborough, UK, User Manual, 100 pp., Issued: 6.6.18, 2018.

de Haij, M., Wauben, W., and Baltink, H. K.: Determination of mixing layer height from ceilometer backscatter profiles, in: Remote Sensing of Clouds and the Atmosphere XI, edited by Slusser, J. R., Schäfer, K., and Comerón, A., vol. 6362, p. 63620R, SPIE, https://doi.org/10.1117/12.691050, 2006.

EASA: European Union Aviation Safety Agency Easy Access Rules for Standardised European Rules of the Air (SERA), European Union Aviation Safety Agency, EASA Headquarters, Cologne, Germany, https://www.easa.europa.eu/en/document-library, EASA eRules SERA, EASA Document Library, Revision from December 2024 − Available in pdf, online and XML format, 2024.

EASA: European Union Aviation Safety Agency Easy Access Rules for Air Operations, European Union Aviation Safety Agency, EASA Headquarters, Cologne, Germany, 22 edn., https://www.easa.europa.eu/en/document-library, EASA eRules Air Operations, EASA Document Library, Revision from February 2025 − Available in pdf, online and XML format, 2025.

Eberhard, W. L.: Cloud Signals from Lidar and Rotating Beam Ceilometer Compared with Pilot Ceiling, J. Atmos. Oceanic Technol., 3, 499–512, https://doi.org/10.1175/1520-0426(1986)003<0499:CSFLAR>2.0.CO;2, 1986.

Ferguson, J. A. and Stephens, D. H.: Algorithm for inverting lidar returns, Appl. Opt., 22, 3673–3675, https://doi.org/10.1364/AO.22.003673, 1983.

Gaumet, J. L., Heinrich, J. C., Cluzeau, M., Pierrard, P., and Prieur, J.: Cloud-Base Height Measurements with a Single-Pulse Erbium-Glass Laser Ceilometer, J. Atmos. Oceanic Technol., 15, 37–45, https://doi.org/10.1175/1520-0426(1998)015<0037:CBHMWA>2.0.CO;2, 1998.

Görsdorf, U., Mattis, I., Pittke, G., Bravo-Aranda, J. A., Brettle, M., Cermak, J., Drouin, M.-A., Geiß, A., Haefele, A., Haefelin, M., Hervo11, M., Kominková, K., Leinweber, R., Lehmann, V., Müller, G., Münkel, C., Pattantyus-Abraham, M., Pönitz, K., Wagner, F., and Wiegner, M.: The ceilometer inter-comparison campaign CeiLinEx2015 − Cloud detection and cloud base height, in: Technical Conference on Meteorological and Environmental Instruments and Methods of Observation (TECO), Madrid, Spain, Extended Abstract, 2016.

HH-WeatherMast: The Hamburg Weather Mast, https://wettermast.uni-hamburg.de/frame.php?doc=MessanlageEng.htm, University of Hamburg, last access: 24 September 2025.

ICAO: Manual of Runway Visual Range Observing and Reporting Practices, International Civil Aviation Organization, ICAO Headquarters, Montréal, Canada, 3 edn., https://amc.namem.gov.mn/wp-content/uploads/ICAO/19.%209328_cons_en_2018.pdf?_t=1638837866, Doc 9328, Appendix B-2, AN/908, 2005.

https://doi.org/10.5194/egusphere-2026-1696
Preprint. Discussion started: 19 May 2026

ICAO: Annex 3 – Meteorological Service for International Air Navigation, Part I – Core SARPs, Part II – Appendencies and Attachements, International Civil Aviation Organization, ICAO Headquarters, Montréal, Canada, 20 edn., ISBN 978-92-9258-482-5, https://www.bazl.admin.ch/bazl/en/home/themen/legislation/anhaenge-icao.html, Amendment 81, AN 3, 2018.

ICAO: Annex 6 – Operation of Aircraft, Part I, International Commercial Air Transport – Aeroplanes, International Civil Aviation Organization, ICAO Headquarters, Montréal, Canada, 12 edn., ISBN 978-92-9265-871-7, https://www.bazl.admin.ch/bazl/en/home/themen/legislation/anhaenge-icao.html, Amendment 49, AN 6-1, 2022.

ICAO: Rules of the Air, Annex 2 to the Convention on International Civil Aviation Organization, International Civil Aviation Organization, ICAO Headquarters, Montréal, Canada, 11 edn., Amendment 48, AN2, 2024a.

ICAO: Manual of All-Weather Operations, International Civil Aviation Organization, ICAO Headquarters, Montréal, Canada, 5 edn., https://www.unitingaviation.com/publications/9365/, Doc 9365, Manual to the Convention on ICAO, 2024b.

Illingworth, A. J., Cimini, D., Haefele, A., Haeffelin, M., Hervo, M., Kotthaus, S., Löhnert, U., Martinet, P., Mattis, I., O'Connor, E. J., and Potthas, R.: How Can Existing Ground-Based Profiling Instruments Improve European Weather Forecasts?, Bull. Am. Meteorol. Soc., 100, 605–619, https://doi.org/10.1175/BAMS-D-17-0231.1, 2019.

ISO 28902-4: Air Quality – Environmental Meteorology – Part 4: Ground-based Remote Sensing of Meteorological Parameters by Particle Backscatter Lidar, International Organization for Standardization, Vernier, Geneva, Switzerland, https://www.iso.org/standard/85502.html, ISO/DIS 28902-4:2025(en), expected publication 22 November 2025 (last access: 10 November 2025), 2025.

Klaus, D. and Görsdorf, U.: Subset of Ceilometer campaign Hansestadt Hamburg (CircaHH) data, Zenodo, v1.0, https://doi.org/10.5281/zenodo.20134337, 2026.

Klett, J. D.: Stable analytical inversion solution for processing lidar returns, Appl. Opt., 20, 211–220, https://doi.org/10.1364/AO.20.000211, 1981.

Lewis, H., Bowyer, J., Broad, A., Chamberlain-Clay, A., Jones, C., Chan, S., Kahraman, A., and Morcrette, C.: Using machine learning to find cloud-base height: a didactic challenge, Weather, 77, 391–395, https://doi.org/https://doi.org/10.1002/wea.4163, 2022.

Lufft: Lufft CHM15k Ceilometer, OTT HydroMet, Fellbach GmbH, Gutenbergstraße 20, Fellbach, Germany, https://www.lufft.com/resources/, User Manual, R19/03-2022, 77 pp., 2022a.

Lufft: Lufft CHM8k Ceilometer, OTT HydroMet, Fellbach GmbH, Gutenbergstraße 20, Fellbach, Germany, https://www.lufft.com/resources/, User Manual, R2.2/10-2022, 76 pp., 2022b.

Mulders, J. M.: Algorithm for inverting lidar returns: comment, Appl. Opt., 23, 2855–2856, https://doi.org/10.1364/AO.23.002855, 1984.

Reichardt, J., Wandinger, U., Klein, V., Mattis, I., Hilber, B., and Begbie, R.: RAMSES: German Meteorological Service autonomous Raman lidar for water vapor, temperature, aerosol, and cloud measurements, Appl. Opt., 51, 8111–8131, https://doi.org/10.1364/AO.51.008111, 2012.

Spänkuch, D., Hellmuth, O., and Görsdorf, U.: What is a Cloud? Toward a More Precise Definition, Bull. American Meteorol. Soc., 103, E1894–E1929, https://doi.org/10.1175/BAMS-D-21-0032.1, 2022.

Stoelinga, M. T. and Warner, T. T.: Nonhydrostatic, Mesobeta-Scale Model Simulations of Cloud Ceiling and Visibility for an East Coast Winter Precipitation Event, J. Appl. Meteorol., 38, 385–404, https://doi.org/10.1175/1520-0450(1999)038<0385:NMSMSO>2.0.CO;2, 1999.

Vaisala: USER'S GUIDE Visibility Sensor PWD10/20, Vaisala, Vaisala Oyj, P.O. Box 26, Helsinki, Finland, User Manual, M210541EN-B, 98 pp., 2004.

https://doi.org/10.5194/egusphere-2026-1696
Preprint. Discussion started: 19 May 2026

Vaisala: USER GUIDE Ceilometer LD40, Vaisala, Vaisala Oyj, P.O. Box 26, Helsinki, Finland, User Manual (in German), M210256de-C, 133 pp., 2005.

Vaisala: USER'S GUIDE Vaisala Ceilometer CL31, Vaisala, Vaisala Oyj, P.O. Box 26, Helsinki, Finland, User Manual, M210482EN-D, 138 pp., 2009.

van Tricht, K., Gorodetskaya, I. V., Lhermitte, S., Turner, D. D., Schween, J. H., and van Lipzig, N. P. M.: An improved algorithm for polar cloud-base detection by ceilometer over the ice sheets, Atmos. Meas. Tech., 7, 1153–1167, https://doi.org/10.5194/amt-7-1153-2014, 2014.

Vande Hey, J. D.: Design, Implementation and Characterisation of a Novel Lidar Ceilometer, Ph.D. thesis, Loughborough University, Loughborough, UK, https://hdl.handle.net/2134/11853, 2013.

Vande Hey, J. D.: A Novel Lidar Ceilometer: Design, Implementation and Characterisation, Springer Theses, Springer International Publishing AG, Cham, Switzerland, 1 edn., ISBN 978-3-319-12612-8 (Print), 978-3-319-12613-5 (Online), https://doi.org/10.1007/978-3-319-12613-5, 158 pp., 2015.

Vogt, F. P. A., Foresti, L., Regenass, D., Réthoré, S., Tarin Burriel, N., Bibby, M., Juda, P., Balmelli, S., Hanselmann, T., du Preez, P., and Furrer, D.: ampycloud: an open-source algorithm to determine cloud base heights and sky coverage fractions from ceilometer data, Atmos. Meas. Tech., 17, 4891–4914, https://doi.org/10.5194/amt-17-4891-2024, 2024.

Wagner, F., Geiß, A., Barnaba, F., Belegante, L., Bellini, A., Buxmann, J., Diémoz, H., Fenner, D., Kotthaus, S., Osborne, M., Ruefenacht, R., de Morales Céspedes, J. R., and van Hove, M.: JND European networks observing the atmospheric boundary layer: Overview, access and impacts – Chapter 2a: Automatic low-power Lidar and Ceilometer (ALC), Zenodo, https://doi.org/10.5281/zenodo.11211873, 2024.

Wandinger, U.: Introduction to Lidar, vol. 102, chap. 1, pp. 1–18, Springer New York, New York, NY, ISBN 978-0-387-25101-1, https://doi.org/10.1007/0-387-25101-4_1, 2005.

Weitkamp, C.: Lidar – Range-Resolved Optical Remote Sensing of the Atmosphere, 456 pp., Springer New York, NY, US, ISBN 978-0-387-40075-4, https://doi.org/10.1007/b106786, 2005.

Wikipedia: Standard RGB, https://en.wikipedia.org/wiki/SRGB, last access: 24 September 2025.

Zinke, J.: Evaluation of cloud base height derived from ceilometer measurements using camera photos of a 300 m tall mast – The weather mast as cloud ruler, BSc. thesis (in German), 49 pp., University of Hamburg, Hamburg, Germany, 2016.